



Degree project in Civil Engineering

Second cycle, 30 credits

# Back analysis of rock mass properties in the regional fault zone under Lake Mälaren

JIAQI LIU

# **Back analysis of rock mass properties in the regional fault zone under Lake Mälaren**

JIAQI LIU

Master Thesis, 2021  
KTH Royal Institute of Technology  
School of Architecture and the Built Environment  
Department of Civil and Architectural Engineering  
Division of Soil and Rock Mechanics  
SE-100 44, Stockholm, Sweden



## **Abstract**

The properties of the surrounding rock mass in underground projects have significant impacts on the design and construction. However, it is quite challenging to evaluate rock mass properties due to the great uncertainties of the geological conditions. Besides, even if techniques of field test have obtained a well development, the high expense of tests and scattering results always make it difficult to cover a large domain in a complex project. In recent years, because of the maturity of numerical analysis as well as the wide use of tunnel deformation measurements, displacement-based back analysis has become a popular and effective indirect method to estimate rock mass properties.

The main purpose of this thesis was to perform a displacement-based back analysis on the in-situ stress ratio and Young's modulus of the exploratory tunnel BP201, which constitutes the passage under the Lake Mälaren in the Stockholm Bypass project. The back analysis was carried out using the Pattern search method and the Simplex method. The error function was built according to the least square method, and the commercial finite element software Plaxis 2D was used to calculate theoretical deformations. Moreover, a sensitivity analysis was performed to study the influence of starting point and how other numerical model parameters affects the results of the back analysis.

The two optimization algorithms used in this study provided an in-situ stress ratio and Young's modulus with close estimations to the measured deformations. For the specific problem analysed in this thesis, it was found that the Simplex method was more suitable than the Pattern search method. It was also concluded that a better choice of starting point can improve the precision and efficiency of the back analysis.

**Keywords:** Rock mass properties, back analysis, tunnel deformation, optimization algorithm, numerical analysis.

## Sammanfattning

Bergmassans egenskaper har en stor påverkan vid dimensioneringen och utformningen av förstärkningen i tunnlar och vid indelningen av uttagssekvenser vid tunneldrivning. Det är emellertid svårt att utvärdera bergmassans egenskaper till följd av stora osäkerheter i de geologiska förhållandena. Även om tekniker för provning i fält har utvecklats är de relativt kostsamma och det är svårt att täcka in hela den geologiska domänen i stora projekt. På senare år har utvecklingen av numeriska metoder och deformationsmätningar i tunnlar möjliggjort bestämning av bergmassans egenskaper genom deformationsbaserad bakåtanalys.

Syftet med detta examensarbete var att utföra en deformationsbaserad bakåtanalys av in-situ spänningstillståndet och bergmassans elasticitetsmodul i bypassstunneln BP 201 under passagen av sjön Mälaren i Stockholm, vilket är en del av projektet Förbifart Stockholm. I bakåtanalysen användes metoderna "the Pattern Search Method" och "the Simplex Metod". Minsta kvadratmetoden användes som felfunktion. Tvådimensionella numeriska beräkningar av deformationerna i tunneln utfördes med det finita elementprogrammet Plaxis 2D. En känslighetsanalys gjordes för att studera inverkan på resultatet vid val av startpunkt i bakåtanalysen och hur osäkerheter i övriga parametrar påverkade resultatet.

De två optimeringsalgoritmerna som användes i denna studie resulterade i in-situ spänningar och en elasticitetsmodul som genererade beräknade deformationer nära de uppmätta. För det studerade problemet i detta arbete var "the Simplex Method" lämpligare att använda än "the Pattern Search Method". Genom att välja ett lämpligare startvärde kunde också precisionen och effektiviteten i bakåtanalysen förbättras.

**Nyckelord:** Bergmassans egenskaper, bakåtanalys, tunneldeformation, optimeringsalgoritm, numerisk analys.

## **Preface/Acknowledgements**

At this point, I will finish the thesis of my master program at KTH Royal Institute of Technology. The idea of this thesis was proposed by AECOM Nordic. I want to express my thanks to all the talented engineers at AECOM Nordic for their care and kindness towards a freshman in this industry. I would like to thank my supervisor Francisco Ríos Bayona for his teaching and great patience with endless questions during this period. Especially, I would like to thank my examiner Fredrik Johansson and supervisor Björn Stille for their efforts. I really appreciated their guidance and suggestions on my thesis and final presentation. They also offered invaluable encouragement to me during the toughest time in quarantine.

Finally, thank you for the supports to my classmates, friends and family!

Stockholm, February 2021

*Jiaqi Liu*

# Nomenclature

## Abbreviations

AI	Artificial Intelligence
NATM	New Austrian Tunneling Method
Q	Tunnel Quality Index
RMR	Rock Mass Rating

## Latin Symbols

$E$	Young's modulus	[GPa]
$F_y$	Yield force	[kN]
$R_{inter}$	Interface factor	
$c$	Cohesion	[kPa]
$e_j$	Coordinate direction	
$f_{cc}$	Compressive strength of shotcrete	[MPa]
$f_j$	Results of numerical analysis in error function	
$f(x)$	Error function	
$f_y$	Yield strength	[MPa]
$k_0$	Stress ratio of horizontal stresses over vertical stresses	
$m$	The number of measurement data in error function	
$p_k$	Initial pressure	[MPa]
$t$	Thickness of shotcrete	[mm]
$u_j$	Measurement value in error function	
$u_i$	Initial tunnel deformation	[mm]
$u_m$	Measured tunnel deformation	[mm]
$u_{tot}$	Total tunnel deformation	[mm]
$u_x$	Horizontal displacement in Plaxis	[mm]
$u_y$	Vertical displacement in Plaxis	[mm]
$ u $	Absolute displacement in Plaxis	[mm]
$\bar{x}$	Middle point of line segment in simplex	
$x_n$	Variables to be optimized	
$\mathbf{x}^{(j)}$	Base point in pattern search method	
$\mathbf{x}^{(n)}$	Vertices of simplex in an (n-1)-dimensional space	
$\mathbf{y}^{(j)}$	Starting point of exploratory move	

## Greek Symbols

$\Sigma M_{stage}$	Total multiplier	
$\alpha_1$	Acceleration factor	
$\alpha_2$	Reflection coefficient	
$\beta$	Proportion of load carried by tunnel support	
$\beta'$	Contraction factor	
$\gamma$	Unit weight of material	[kN/m <sup>3</sup> ]
$\gamma'$	Expansion factor	
$\delta$	Step size of exploratory move	
$\epsilon$	Mean square error	
$\nu$	Poisson's ratio	
$\sigma_{cm}$	Compressive strength of rock mass	[MPa]
$\sigma_{tm}$	Tensile strength of rock mass	[MPa]
$\phi$	Diameter of rock bolts	[mm]
$\varphi$	Friction angle	[ ° ]
$\hat{\lambda}$	Vector of parameters to be predicted	
$\psi$	Dilatancy angle	[ ° ]

# Content

<b>1. Introduction</b> .....	<b>1</b>
1.1. Background .....	1
1.2. Objective .....	2
1.3. Disposition.....	3
1.4. Limitations.....	4
<b>2. Literature review</b> .....	<b>5</b>
<b>3. Methodology</b> .....	<b>11</b>
3.1. Numerical analysis.....	11
3.2. Error function .....	15
3.3. Optimization algorithm .....	16
3.3.1. Pattern search method.....	16
3.3.2. Simplex method .....	19
<b>4. Case study</b> .....	<b>23</b>
4.1. Introduction to Stockholm Bypass.....	23
4.2. Geological conditions.....	24
4.3. Tunnel geometry and initial support .....	27
4.4. Deformations in the tunnel.....	30
4.5. Numerical analysis.....	35
4.5.1. Description of numerical model.....	35
4.5.2. Estimation of <i>Mstage</i> .....	37
<b>5. Results</b> .....	<b>40</b>
5.1. Results of numerical analysis.....	40
5.2. Results of back analysis .....	41
5.2.1. Optimization with the Pattern Search Method.....	41
5.2.2. Optimization with the Simplex Method.....	43
<b>6. Discussion</b> .....	<b>47</b>
6.1. Comparison between two optimization algorithms .....	47
6.2. Influence of <i>Mstage</i> .....	49
6.3. Influence of starting point.....	53
<b>7. Conclusions</b> .....	<b>56</b>
<b>8. References</b> .....	<b>58</b>

# 1. Introduction

## 1.1. Background

Determination of rock mass properties is an important task in the design and construction of underground structures. As one of the most critical mechanical properties of rock mass, the Young's modulus gives knowledge about the magnitude and characteristic of the rock mass deformation due to changes in the stress field [1].

The in-situ stress is a natural state of stress imposed on initial undisturbed rock mass. As one of the fundamental conditions for design and stability analysis of rock excavation projects, the in-situ stress field has impacts on the study of rock mass deformation and failure [2].

In-situ test methods such as the plate loading test and jacking test are common to determine the deformation modulus of the rock mass. However, it is not feasible to perform field test extensively in the whole construction area because it is time consuming and expensive. The results of the test are also sometimes not reliable. Several empirical methods based on rock mass classification schemes such as Rock Mass Rating (RMR) and the Tunnel Quality Index (Q) [3] are proposed in order to overcome the drawbacks of the field test, but the assumption of an isotropic rock mass in these methods reduces the reliability of these methods in highly jointed rock masses [4]. A similar problem exists in the prediction of in-situ stresses. At shallow depth, in-situ stresses are often influenced by the topography of the rock surface and near surface weathering [5]. Besides, the measurement points of in-situ stresses are distributed in the entire area for the reasons of expense, which also leads to high uncertainties in the measurement of in-situ stresses.

Back analysis is a method frequently applied in geotechnical and structural engineering in recent decades. The procedure of back analysis can be summarized as using field measurement (in most cases displacements and stresses) in order to obtain input material parameters [6]. Back analysis problem can also be described as: define the values of unknown parameters which are adopted in the stress analysis of the geotechnical system and these unknown parameters should lead to results as close as possible to the available measurement data [7].

Displacements tend to be chosen as measurement data in back analysis because of the maturity of underground instrumentation techniques. The convergence of the tunnel during and after construction is usually monitored with extensometers and optical system, which can deliver precise results. Moreover, the tremendous progress of computer science such as artificial intelligence (AI) and neural network, together with the wide application of numerical analysis, boosts the development of optimization algorithms and provides many new solutions to back analysis problems, which improve the preciseness and efficiency of back analysis methods.

The advantage of back analysis methods compared to field tests consists in the utilization of measurement data, which is the direct consequence of real values of rock mass parameters. However, it is notable that back analysis is based on optimization algorithms. Hence, the choice of algorithms has a great influence on the efficiency and preciseness of the back analysis.

## **1.2. Objective**

This study aims to use back analysis method to predict Young's modulus and stress ratio of horizontal stresses over vertical stresses in the regional fault zone under the Lake Mälaren in the Stockholm Bypass project. Direct approach and two kinds of classical optimization algorithms are adopted in this analysis.

The main objectives are to:

- Summarize geological information in the regional fault zone and calculate initial tunnel deformations with a numerical method.
- Based on measured deformation and the results of numerical analysis, perform a back analysis on Young's modulus and stress ratio with classical optimization algorithms.
- Perform sensitivity analysis and compare the efficiency of two classical optimization algorithms.

### 1.3. Disposition

This master thesis is divided into 7 chapters and starts in Chapter 2 by briefly reviewing practical applications of back analysis in previous studies of other researchers. Chapter 3 explains the method used in this master thesis. This chapter also contains the procedure and theory of numerical analysis with Plaxis 2D, the concept of the error function based on the least square method and the principle of optimization algorithms such as the Pattern Search Method and the Simplex Method.

Chapter 4 deals with the geometry and geological conditions of the exploratory tunnel BP201, including mapped fractures, excavation sequences and rock support. This chapter also focuses on the monitoring system and deformation measurements in the tunnel. The description of the numerical model of BP201 forms the last section of this chapter.

Chapter 5 presents the results of numerical analysis and the results of the search paths of optimization with two different algorithms. In Chapter 6, the preciseness and efficiency of the back analysis are discussed and compared with respect to the Pattern Search Method and the Simplex Method. In addition, the sensitivity of the back analysis to the parameter  $\sum M_{stage}$  and search starting point is studied. Finally, the conclusions of this master thesis are drawn and future work is proposed in Chapter 7.

## 1.4. Limitations

Classical optimization algorithms applied in this study conduct a local search for the minimum of the error function instead of searching in the entire parameter space. It is very common that the error function in a complicated geotechnical problem is highly non-linear and has several local minimums. Therefore, different search starting points will lead to different optimum solutions. It is difficult to check if the obtained solutions are the global minimum. In this case, the uncertainty can be reduced by performing several runs of the optimization process with different initial guesses and analyze the outputs [6].

The iterations with classical optimization algorithms are always a time-consuming process, which means iterative procedure requires a large amount of computations. In most cases, the algorithms are programmed within the numerical software to improve the efficiency of the computation. However, in this thesis, for the sake of simplicity, the iterations are conducted with Plaxis 2D and Excel separately, which will increase the time of computation.

## 2. Literature review

In general, any back analysis problem can be solved in two different approaches that are referred to as the inverse approach and the direct approach [7].

In the inverse approach, information from field measurements are used as input data and unknown parameters appear as output data in an equation system. The formulation is just derived reversely from those adopted in ordinary stress analysis. Furthermore, in the inverse approach, the number of monitoring values is required to exceed the number of unknown parameters so that the equation set has more equations than unknowns. An inverse approach based on finite element formulation was applied by Sakurai [8] to analyze the initial state of stresses and Young's modulus with measured displacements. In this study, Poisson's ratio and the vertical initial stress were assumed as known quantities. The rock mass around the excavation was also assumed as linear, isotropic and elastic.

The inverse approach is characterized by a high efficiency. It needs less time to converge but has the limitation of computational issues. For example, in order to invert the governing equations, and when a numerical model is used, it demands the access to the software code which is not possible to obtain most of the time [6].

In order to perform back analysis with the direct approach, it is necessary to have [9]:

- A representative numerical model that can determine the stress/strain field in the rock mass.
- An error function.

- An algorithm which can reduce the difference between the results of the numerical calculation and the results of in-situ measurements.

The numerical model used in the direct approach is the same as the model utilized in normal stress analysis. The error function describes the discrepancy between in-situ measured values and numerically computed values. An iteration can be conducted by an optimization algorithm and the aim of this procedure is to minimize the error function so that it can converge. In the direct approach, no formulation is required like in the inverse approach. The direct approach has a more general validity and is more suitable to use for a range of different back analysis problems [7].

Miranda performed a state-of-the-art review of optimization algorithms [6]. Normally, two types of algorithms are often applied to minimize the error function: classical optimization algorithms and optimization methods from the evolutionary computation and artificial intelligence field.

The Simplex method is a kind of frequently used classical optimization algorithm in the displacement-based back analysis. The general search path of the Simplex method in a two-dimensional space is illustrated in Figure 1. The simplex in a two-dimensional space is a triangle, and values of the error function at vertices are minimized by changing the shape of the simplex stepwise. Cividini and coworkers applied the Simplex method to a weak rock layer resting on a sound rock bed to determine the Young's modulus of two kinds of rock masses and the values of the parabolic load distribution [7].

Another common classical optimization technique is the univariate optimization algorithm. In the univariate method, the search path is along the line parallel to the coordinate axis because only one variable is changed at one time. Starting from a base point, one variable is changed and all the other variables are fixed. After optimization of one variable in the first step, a new base point can be obtained. Then, the search is performed in another direction by changing the value of another variable which is fixed in previous step, while the remaining ones are fixed. The

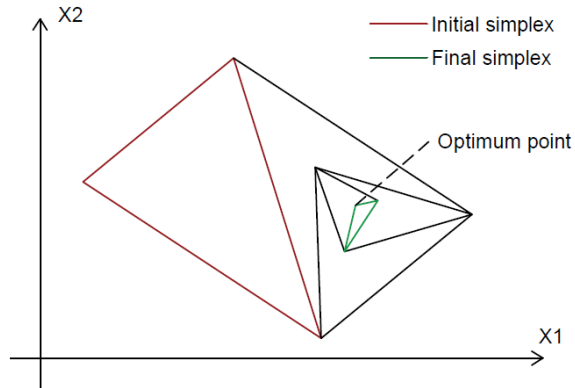


Figure 1: General search path using the Simplex method in a two-dimensional space

first cycle is completed after all variables have been sought successively and afterwards the whole search procedure is repeated. This process continues until the change of the variables in any direction will not improve the error function anymore. A general search path of the univariate method in a two-dimensional space is illustrated in Figure 2. Yazdani applied the univariate optimization algorithm in the back analysis of geo-mechanical properties and joints parameters of the Siah Biseh pumped storage project using both continuum and discontinuum models [10].

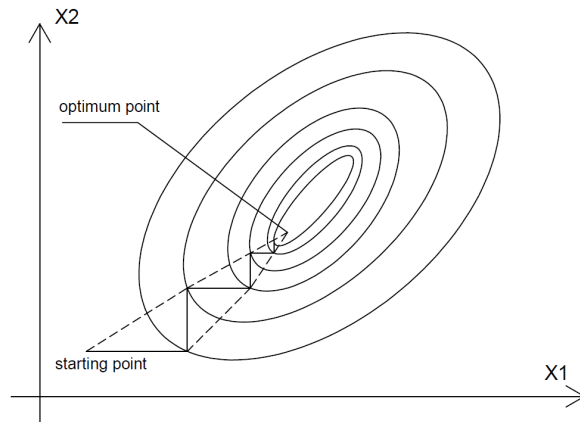


Figure 2: General search path using the univariate method in a two-dimensional space

The use or not of the first and second derivatives of the error function distinguishes different types of optimization algorithms and also determines their applicability. The utilization of the first and second derivatives can improve the efficiency of the optimization algorithms. However, the error function is sometimes not differentiable or the computation of gradients requires much more computational time [6].

The correctness of numerical models influences the results of back analysis in the direct approach. The probability for the error function to converge is higher if the numerical and constitutive model are able to describe the ground behavior accurately. The quantity and the quality of measurement data also have an impact on the results of the optimization.

The classical optimization algorithms are restricted sometimes because the iterations are always a time-consuming process, which means that an iterative procedure requires a large amount of computations. For example, in the study of Jeon and Yang [11], two unknown parameters brought 6-8 iterations for the error function to converge. In most cases, the classical optimization algorithms are suitable for the back analysis of a maximum of two to three parameters. Therefore, it is important to carry out a sensitivity analysis before the back analysis to determine the parameters that have the largest influence on the results.

Another limitation of the classical optimization algorithms is the local search for the minimum of the error function instead of the search in the entire parameter space. Highly non-linear and several local minimums are always characterizations of the error function in a complex geotechnical problem. Thus, back analysis starting from different initial unknown parameters may result in different optimum solutions. It is difficult to check if the obtained solutions are the global minimum or not. One possible strategy to overcome this limitation is to perform several rounds of optimization processes, starting from different initial points. If each searching path reaches the same optimum point, the existence of the global optimum point can be verified [6].

In order to overcome the weaknesses of classical optimization algorithms, the recent development of artificial intelligence arouses the related metaheuristic optimization algorithms such as evolutionary

algorithms. The new displacement-based back analysis proposed by Feng [12] combined a neural network, an evolutionary calculation and numerical analysis techniques, which is capable of handling the non-linear relation between displacement and rock mechanical parameters. The neural network adopted genetic algorithms to search rock mechanical parameters in the entire variable space to ensure the optimum solutions in the global range.

Evolutionary algorithms are inspired by Darwin's Theory of natural selection and survival of the fittest, which simulates the natural election of species in biological systems [13]. Evolutionary algorithms are distinguished from conventional optimization algorithms by searching for the optimum in the entire parameter space. The values of the error function calculated sequentially under different parameter sets are compared with each other. Continuity and convexity of the error function is unnecessary in the evolutionary algorithms. Furthermore, only information about the objective function and constraints is required to perform the search. Another difference between evolutionary algorithms and conventional ones is that optimization starts from a series of solutions which evolves over time instead of from individual to individual [6].

Parametric studies can substitute direct back analysis when the computational time is extremely long. In the Stockholm Odenplan station project, deformations of the rock mass were measured with three extensometers located in the tunnel roof. The measured deformations were suitable to conduct a direct back analysis, but the 3DEC model in this case, under elasto-plastic conditions, took two to three weeks for one single run. The computation time would reach six months if only two parameters were optimized in the back analysis for this project [5]. Therefore, a parametric study was performed instead of a complete back analysis.

In the parametric study, no optimization algorithms are applied. The deformation from numerical analysis are just compared with measured deformation. If the deformations of the numerical model are in good agreement with measured displacements, the correctness of the rock

mechanical parameters are assumed to be confirmed. This methodology was also applied in the Shimizu Tunnel No.3 project to study the behavior of the wide tunnel geometry under various conditions [14]. In this study, the results of the simulations using UDEC and the convergence-confinement method were comparable to the measurement of tunnel deformations and support loads.

### 3. Methodology

The procedure of the back analysis in this study is illustrated in Figure 3.

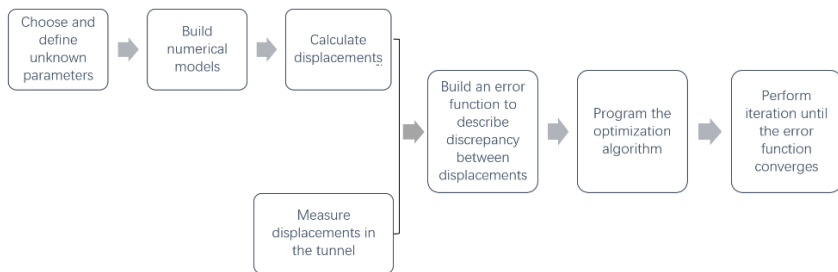


Figure 3: Flowchart of back analysis

#### 3.1. Numerical analysis

The numerical model of Bypass tunnel 201 is built with Plaxis 2D, which is a widely-used numerical analysis software in the field of geotechnical engineering. The modelling procedure can be illustrated in Figure 4.

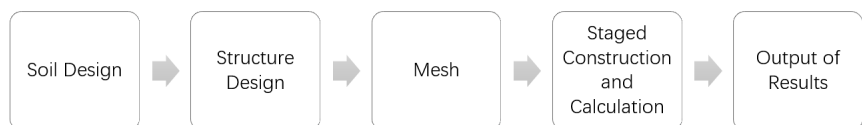


Figure 4 Procedure of the numerical analysis with Plaxis 2D

- **Soil design and ground water**

The dimension of soil layers should be large enough to reduce the impacts on the results of numerical model. Normally, the distance

between the tunnel center and the boundary should be larger than three times the tunnel diameter.

One of the methods to define soil and rock mass conditions in Plaxis 2D is to create boreholes. In this case, only one borehole is needed to define the rock mass because there are no fluctuations of height among different rock mass layers.

Without considering the influence of ground water flow in the rock mass, the numerical analysis is assumed to be performed in dry conditions (i.e. total stress analysis), and the 20 m water in Lake Mälaren above the subsea tunnels is modelled as a uniformly distributed load for simplicity.

The rock mass behavior is described with the Mohr-Coulomb failure criterion and an elastic perfectly plastic rock mass. The Mohr-Coulomb model involves five input parameters, i.e. Young's modulus  $E$  and Poisson's ratio  $\nu$  for rock elasticity; cohesion  $c$ , friction angle  $\varphi$  and dilatancy angle  $\psi$  for rock plasticity. For the "Drainage type", the "Drained condition" is suitable in this case because the influence of the ground water is insignificant and there is assumed that no pore pressure exists in the rock mass close to the tunnel that influence the deformations.

- **Structure design**

The 2D numerical model is a cross section perpendicular to the advance direction of the Bypass 201 tunnel. The modelled section is located at section 12/505. The geometry of the cross section and the corresponding rock bolts are imported into Plaxis 2D directly from AutoCAD.

In order to simulate the shotcrete around the tunnel, plate elements are created on walls and ceiling, as shown in Figure 5. A positive interface is applied outside the walls and ceiling to simulate the interaction between rock and shotcrete. The interface behavior is defined with an elastic-plastic model. The interface allows the relative displacement such as slipping and gapping between rock and shotcrete. The relative displacement depends on the parameter  $R_{inter}$ , which represents the stiffness and strength properties of the interface [15].  $R_{inter}$  can be calculated automatically from the material properties of the adjacent rock

cluster, or it can also be set manually. In many cases,  $R_{inter}$  is difficult to estimate, and in this study,  $R_{inter}$  is set to be 0.8.

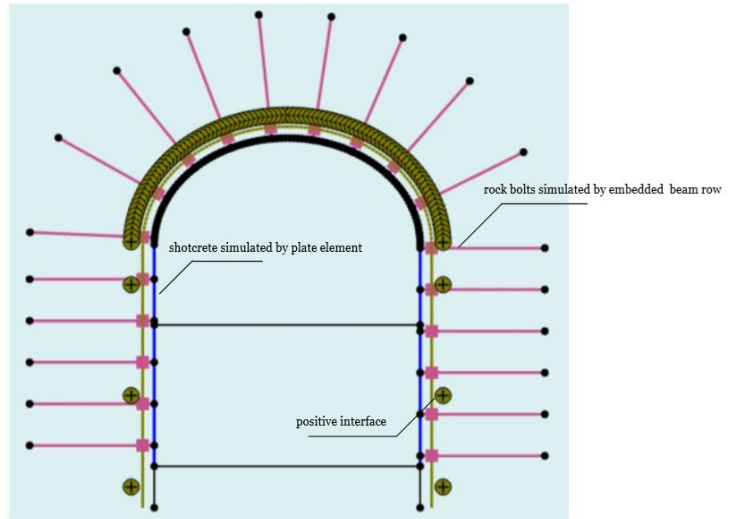


Figure 5 Plate element and embedded beam row in the numerical model

Rock bolts are simulated with an embedded beam row in Plaxis 2D. The top of the embedded beam row element is connected to the plate element around the tunnel, as shown in Figure 5. The connection point is set as rigid because the top of embedded beam row and the rock at this point share the coupled displacement and rotation.

- **Mesh**

The mesh is generated with 15-noded elements globally in this study. Plaxis 2D automatically refines the mesh around the structural elements. In order to obtain more accurate results in the area with stress concentrations and larger deformations, the mesh is further refined in a rectangular space around the tunnel, as shown in Figure 6. The coarseness of the mesh can also be set manually with a coarseness factor.

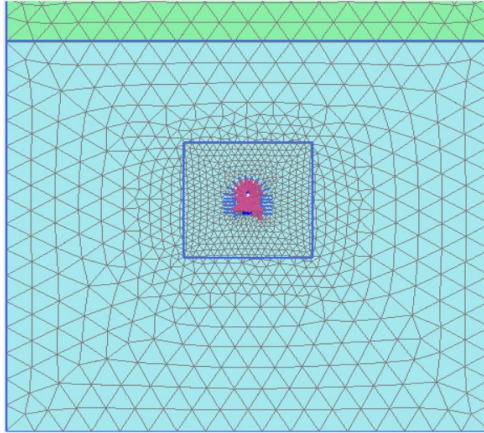
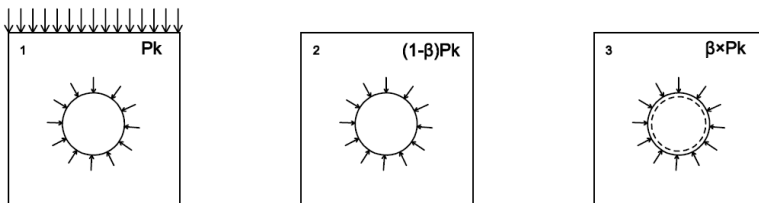


Figure 6 Further refined mesh area around the tunnel

- **Staged construction and calculation**

The tunnel constructed is supported by sprayed concrete lining and rock bolts. For stability and production reasons, the tunnel face is split into top heading and bench. In the tunnel excavation, three-dimensional arching effect occurs within the soil and deformations occurs around the unsupported tunnel face [15]. Therefore, staged construction must be simulated properly in order to make numerical analysis conform to the reality.

The method to realize staged construction in Plaxis 2D is derived from the  $\beta$  – *method*, one of the methods to analyze tunnels constructed according to NATM [15]. The idea of the  $\beta$  – *method* is that the initial stress  $p_k$  acting around the location where the tunnel is to be constructed is divided into a part  $(1 - \beta)p_k$  that is applied to the unsupported tunnel and a part  $\beta p_k$  that is applied to the supported tunnel, as shown in Figure 7.

Figure 7 Principles of the  $\beta$ -method

Specifically, staged construction in Plaxis 2D is controlled by a total multiplier  $\sum M_{stage}$ . The total multiplier is zero at the start of the staged construction calculation. When the tunnel is excavated without tunnel support activated,  $\sum M_{stage}$  is a value less than 1, which is equivalent of  $(1 - \beta)$  in the  $\beta$  - method. Then, after the tunnel is supported with shotcrete and rock bolts, this multiplier is expected to reach the ultimate level (generally 1.0) at the end of the calculation phase.

The value of  $\sum M_{stage}$  can be determined with the ground reaction curve from Plaxis 2D and the empirical value of tunnel deformation before the activation of support. The specific procedure of  $\sum M_{stage}$  estimation is illustrated in section 4.5.2.

### 3.2. Error function

The most commonly used error function is based on the least square method [16]. It can be defined as:

$$\epsilon = \frac{1}{m} \sum_{j=1}^m \left[ \frac{u_j - f_j(\hat{\chi})}{u_j} \right]^2, \quad (3-1)$$

where  $\epsilon$  is the mean square error,  $\hat{\chi}$  is the vector of  $n$  components of parameters to be predicted,  $u_j$  is the  $j$  measurement value,  $f_j$  is the value from numerical calculations corresponding to the  $j$  measurement and  $m$  is the number of in-situ measurements.

### 3.3. Optimization algorithm

#### 3.3.1. Pattern search method

The pattern search is a specific kind of strategy used in direct search solutions, which was first introduced by Hooke and Jeeves [17]. The Pattern Search Method aims to minimize a function  $f(x)$  of several variables  $x = (x_1, x_2, \dots, x_n)$ , which can be realized by changing the argument  $x$  stepwise until the minimum of  $f(x)$  is reached.

The argument  $x = (x_1, x_2, \dots, x_n)$  of function  $f(x)$  can be regarded as the point in an N-dimensional space. The variation of argument  $x$  can be considered as going from one point to another point along a certain path. This procedure can be defined as a *move*. The *move* will be judged as *success* if the function  $f(x)$  decreases; otherwise, it will be defined as *failure* [17].

There are two types of *move* in the pattern search method. The first type of move is the exploratory move. It is conducted along each coordinate axis of argument  $x = (x_1, x_2, \dots, x_n)$ . The success or failure of the exploratory move can provide information about the location of a new base point and a “pattern”, which indicates a probable direction for the next successful move. The second type of *move* is the pattern move which aims to proceed in the direction acquired in the exploratory move and achieve the minimization of function  $f(x)$ . After the decreasing direction of function (pattern) is decided, a series of exploratory move is conducted to modify the pattern.

The point where the pattern move starts is designated as a base point. Geometrically, the basic idea of the pattern search can be conceived to proceed from one base point to another to ultimately find the “valley” where the minima is located, as shown in Figure 8.

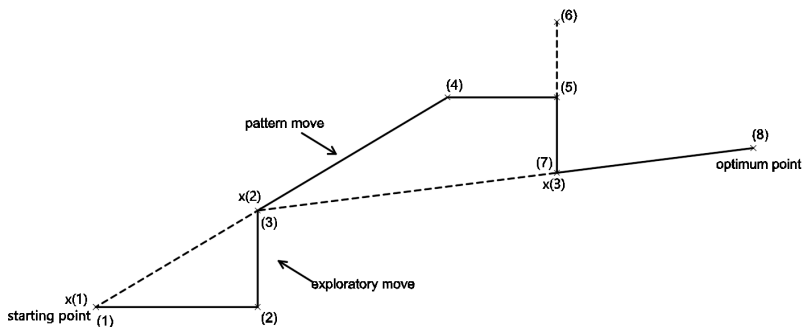


Figure 8 Principles of the Pattern Search Method

The detailed steps of the Pattern Search Method are described as follows: for the function  $f(x), x \in R^n$ , the coordinate direction  $e_j$  represents the direction along which exploratory move is conducted.

$$e_j = (0, \dots, 0, 1, 0, \dots, 0)^T, \quad j = 1, \dots, n,$$

The  $e_j$  in a two-dimensional space is illustrated in Figure 9:

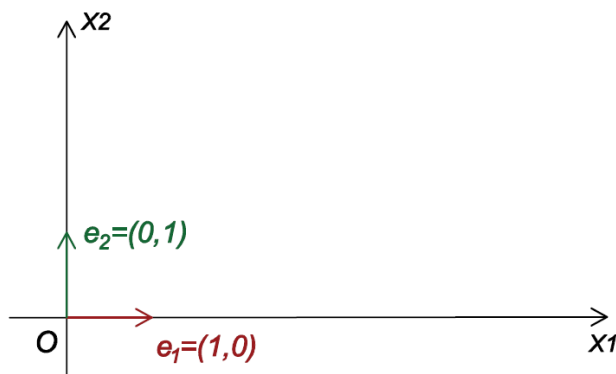


Figure 9 Coordinate direction in a two-dimensional space

Given the initial step size  $\delta$  and acceleration factor  $\alpha$ , choose an initial solution vector  $x^{(1)}$  as the first base point. In the same way,  $x^{(j)}$  represents the base point  $j$ . In each round of exploratory move, the argument is designated as  $y^{(j)}$ , which means  $y^{(j)}$  is the starting point along direction of  $e_j$ , and  $y^{(j+1)}$  is the point updated after the exploratory move along  $e_j$ .

### Exploratory move

Exploratory move starts from  $\mathbf{y}^{(1)} = \mathbf{x}^{(1)}$  along the direction of  $\mathbf{e}_1$ .

If  $f(\mathbf{y}^{(1)} + \delta\mathbf{e}_1) < f(\mathbf{y}^{(1)})$ , the move is successful. Define

$$\mathbf{y}^{(2)} = \mathbf{y}^{(1)} + \delta\mathbf{e}_1 \quad (3 - 2)$$

and start exploratory move from  $\mathbf{y}^{(2)}$  along the direction of  $\mathbf{e}_2$ .

If  $f(\mathbf{y}^{(1)} + \delta\mathbf{e}_1) \geq f(\mathbf{y}^{(1)})$ , the exploratory move along  $\mathbf{e}_1$  fails. Then try the direction of  $-\mathbf{e}_1$ .

If  $f(\mathbf{y}^{(1)} - \delta\mathbf{e}_1) < f(\mathbf{y}^{(1)})$ , the move along  $-\mathbf{e}_1$  is successful. Define

$$\mathbf{y}^{(2)} = \mathbf{y}^{(1)} - \delta\mathbf{e}_1 \quad (3 - 3)$$

and start exploratory move from  $\mathbf{y}^{(2)}$  along  $\mathbf{e}_2$ .

If  $f(\mathbf{y}^{(1)} - \delta\mathbf{e}_1) \geq f(\mathbf{y}^{(1)})$ , the explore along  $-\mathbf{e}_1$  also fails. Define

$$\mathbf{y}^{(2)} = \mathbf{y}^{(1)} \quad (3 - 4)$$

Then, do exploratory move along  $\mathbf{e}_2$  with the same method as above and obtain the point  $\mathbf{y}^{(3)}$ . Follow the same procedure until all the  $n$  coordinate directions are explored and obtain the point  $\mathbf{y}^{(n+1)}$ .

### Pattern move

If  $f(\mathbf{y}^{(n+1)}) < f(\mathbf{x}^{(1)})$ ,  $\mathbf{y}^{(n+1)}$  becomes the new base point and define

$$\mathbf{x}^{(2)} = \mathbf{y}^{(n+1)} \quad (3 - 5)$$

In this case,  $\mathbf{d} = \mathbf{x}^{(2)} - \mathbf{x}^{(1)}$  is a probable direction to decrease the function  $f(\mathbf{x})$ .

Do the pattern move in the direction of  $\mathbf{x}^{(2)} - \mathbf{x}^{(1)}$ , and define the **new**  $\mathbf{y}^{(1)}$  according to eq. (3 - 6).  $\alpha_1$  is the acceleration factor and equal to 1 in most cases.

$$\mathbf{y}^{(1)} = \mathbf{x}^{(2)} + \alpha_1(\mathbf{x}^{(2)} - \mathbf{x}^{(1)}) \quad (3 - 6)$$

After the pattern move, a new round of exploratory move starts from  $\mathbf{y}^{(1)}$ . The exploratory move is still conducted along each coordinate direction and the final point is still designated as  $\mathbf{y}^{(n+1)}$ .

If  $f(\mathbf{y}^{(n+1)}) < f(\mathbf{x}^{(2)})$ , the pattern move is successful and the new base point is designated as  $\mathbf{x}^{(3)} = \mathbf{y}^{(n+1)}$ . Then, the next pattern move will be conducted in the direction of  $\mathbf{x}^{(3)} - \mathbf{x}^{(2)}$ .

If  $f(\mathbf{y}^{(n+1)}) > f(\mathbf{x}^{(2)})$ , both the pattern move and the following exploratory move fail. The simplest way to continue the search would be to return to the base point  $\mathbf{x}^{(2)}$ , reduce the value of the step size  $\delta$  and start over again with a series of exploratory moves and finally establish a new pattern.

The search process will be terminated when the step size is sufficiently small to make sure that the approximation is close enough to the real optimum [17].

### 3.3.2. Simplex method

The Simplex method is another type of direct search method in unconstrained optimization. Simplex is a convex polyhedron with  $n + 1$  vertices in an  $n$ -dimensional space. For example, the line segment is the simplex in one-dimensional space. A triangle is the simplex in the two-dimensional space and a tetrahedron is the simplex in the three-dimensional space.

The Simplex method has the advantage of insensitivity to numerical noise. Besides, the Simplex method only evaluates values of the objective function. The properties of the objective function have a relatively small influence on the results because no specific continuity or other assumptions are required [18].

The basic idea of the Simplex method is different from other direct search methods. In the Simplex method, after the initial simplex is constructed, function values at each vertex of given simplex are calculated. The point with the largest function value is termed as the *worst vertex*, and the point with the smallest function value is designated as the *best vertex*. A better vertex can be obtained by moving vertices according to certain rules (reflection, expansion, contraction and shrink), as shown in Figure 10, and then the worst vertex is replaced with this better vertex in order to construct a new simplex. In this way, the function values at the vertices will approach to the minimum value stepwise.

METHOD

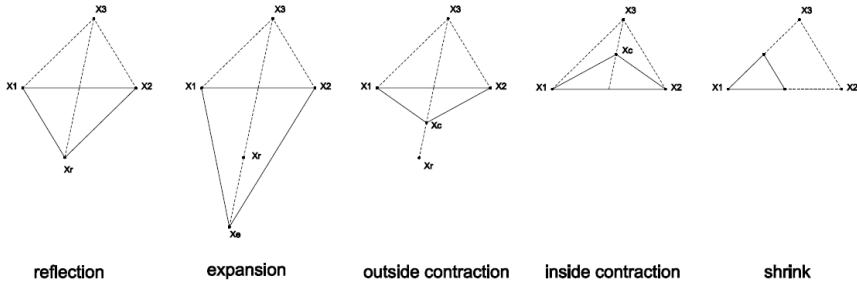


Figure 10 Different conversion rules of the Simplex method in a 2D space

The back analysis in this study concerns two mechanical parameters of the rock mass: the Young’s modulus and the ratio between vertical and horizontal in-situ stresses. Therefore, the optimization with the Simplex method is performed in a two-dimensional space.

The detailed steps of the Simplex method for a function  $f(x_1, x_2)$  are described as follows:

The initial simplex is composed of three noncollinear points  $x^{(1)}$ ,  $x^{(2)}$  and  $x^{(3)}$ , as shown in Figure 11. The worst vertex is designated as  $x^{(3)}$  and the best vertex is designated as  $x^{(1)}$ , namely

$$f(x^{(1)}) < f(x^{(2)}) < f(x^{(3)}) \tag{3 - 7}$$

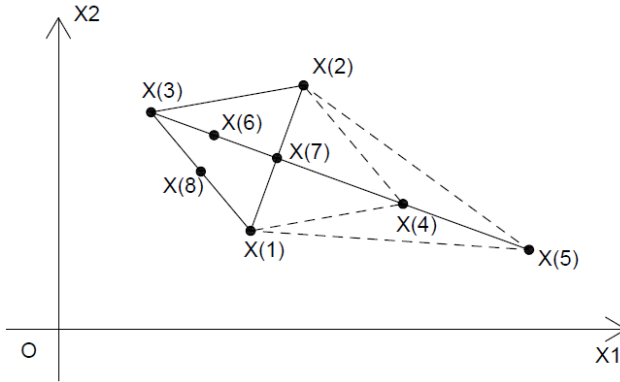


Figure 11 Example of the Simplex method in a 2D space

The worst vertex  $x^{(3)}$  is reflected over the center point of line segment  $x^{(1)}x^{(2)}$

$$\bar{\mathbf{x}} = \frac{1}{2}(\mathbf{x}^{(1)} + \mathbf{x}^{(2)}) \quad (3-8)$$

The vertex obtained after reflection

$$\mathbf{x}^{(4)} = \bar{\mathbf{x}} + \alpha(\bar{\mathbf{x}} - \mathbf{x}^{(3)}) \quad (3-9)$$

$\alpha$  is termed as reflection coefficient and normally equal to 1.

There are three kinds of relationship among  $f(\mathbf{x}^{(4)})$ ,  $f(\mathbf{x}^{(1)})$ ,  $f(\mathbf{x}^{(2)})$  and  $f(\mathbf{x}^{(3)})$  after reflection:

(1) If  $f(\mathbf{x}^{(4)}) < f(\mathbf{x}^{(1)})$ , the direction

$$\mathbf{d} = \mathbf{x}^{(4)} - \bar{\mathbf{x}} \quad (3-10)$$

is favorable to the decrease of objective function. Therefore, expansion is conducted in this direction as

$$\mathbf{x}^{(5)} = \bar{\mathbf{x}} + \gamma'(\mathbf{x}^{(4)} - \bar{\mathbf{x}}), \quad (3-11)$$

where  $\gamma'$  is the expansion factor and  $\gamma' > 1$ .

If

$$f(\mathbf{x}^{(5)}) < f(\mathbf{x}^{(4)})$$

replace  $\mathbf{x}^{(3)}$  with  $\mathbf{x}^{(5)}$ , and a new simplex is made up of  $\mathbf{x}^{(1)}$ ,  $\mathbf{x}^{(2)}$  and  $\mathbf{x}^{(5)}$ .

If

$$f(\mathbf{x}^{(5)}) \geq f(\mathbf{x}^{(4)})$$

the expansion fails. Then, replace  $\mathbf{x}^{(3)}$  with  $\mathbf{x}^{(4)}$  and obtain a new simplex with  $\mathbf{x}^{(1)}$ ,  $\mathbf{x}^{(2)}$  and  $\mathbf{x}^{(4)}$  as vertices.

(2) If the function value at  $\mathbf{x}^{(4)}$  is not less than the worst vertex and is not larger than the middle vertex, namely

$$f(\mathbf{x}^{(1)}) \leq f(\mathbf{x}^{(4)}) \leq f(\mathbf{x}^{(2)})$$

replace  $\mathbf{x}^{(3)}$  with  $\mathbf{x}^{(4)}$ . Vertices  $\mathbf{x}^{(1)}$ ,  $\mathbf{x}^{(2)}$  and  $\mathbf{x}^{(4)}$  form a new simplex.

(3) if  $f(\mathbf{x}^{(4)})$  is larger than the function value at the middle vertex

$$f(\mathbf{x}^{(4)}) > f(\mathbf{x}^{(2)})$$

contraction is conducted. Choose the minimum value of function between vertex  $\mathbf{x}^{(4)}$  and  $\mathbf{x}^{(3)}$

$$f(\mathbf{x}^{(h')}) = \min\{f(\mathbf{x}^{(3)}), f(\mathbf{x}^{(4)})\}, \mathbf{x}^{(h')} \in \{\mathbf{x}^{(3)}, \mathbf{x}^{(4)}\}$$

Then

$$\mathbf{x}^{(6)} = \bar{\mathbf{x}} + \beta'(\mathbf{x}^{(h')} - \bar{\mathbf{x}}) \quad (3-12)$$

$\beta' \in (0,1)$  is designated as contraction factor.  $\mathbf{x}^{(6)}$  is between  $\bar{\mathbf{x}}$  and  $\mathbf{x}^{(h')}$ .

If  $f(\mathbf{x}^{(6)}) \leq f(\mathbf{x}^{(h')})$ , replace  $\mathbf{x}^{(3)}$  with  $\mathbf{x}^{(6)}$  and obtain a new simplex composed of  $\mathbf{x}^{(1)}$ ,  $\mathbf{x}^{(2)}$  and  $\mathbf{x}^{(6)}$ .

If  $f(\mathbf{x}^{(6)}) > f(\mathbf{x}^{(h')})$ , shrink is performed by keeping the worst vertex  $\mathbf{x}^{(1)}$  constant, moving  $\mathbf{x}^{(2)}$  towards  $\mathbf{x}^{(1)}$  in a distance of  $\frac{1}{2}\mathbf{x}^{(2)}\mathbf{x}^{(1)}$  and moving  $\mathbf{x}^{(3)}$  towards  $\mathbf{x}^{(1)}$  in a distance of  $\frac{1}{2}\mathbf{x}^{(3)}\mathbf{x}^{(1)}$

$$\mathbf{x}^{(7)} = \mathbf{x}^{(2)} + \frac{1}{2}(\mathbf{x}^{(1)} - \mathbf{x}^{(2)}) \quad (3 - 13)$$

$$\mathbf{x}^{(8)} = \mathbf{x}^{(3)} + \frac{1}{2}(\mathbf{x}^{(1)} - \mathbf{x}^{(3)}) \quad (3 - 14)$$

A new simplex is formed with vertices  $\mathbf{x}^{(1)}$ ,  $\mathbf{x}^{(7)}$  and  $\mathbf{x}^{(8)}$ .

It has been demonstrated that any new simplex obtained from step (1), (2) and (3) has a vertex at which the function value is not larger than the value at each vertex of the initial simplex. Iteration is performed after obtaining a new simplex until convergence criterion is satisfied.

## 4. Case study

### 4.1. Introduction to Stockholm Bypass

As one of the most important cities in the Nordic countries, Stockholm, is expected to function as the growth engine of Sweden. The meeting of the Baltic Sea and Lake Mälaren in Stockholm gives it numerous waterways, but they also split the city into parts. Currently, Essingeleden is the only major road linking two parts of Stockholm. However, the population of Stockholm region is foreseen to increase by 0.5 million in the future decade. Simultaneously, the larger vehicle volume caused by the population expansion will reduce the safety and sustainability of Essingeleden, and intensify the pressure of the traffic system in Stockholm. The increasing traffic load also accelerates the damage of the roads and leads to larger requirement of repair.

E4 Bypass Stockholm (E4 Förbifart Stockholm in Swedish) is a new route of the European highway (E4), passing the capital of Sweden. Currently, the bypass is under construction. The project starts from the Kungens Kurva interchange in the south of Stockholm and ends at the Häggvik interchange north of Stockholm, as shown in Figure 12. It is planned to be 21 km, and composed mainly of serial underground motorway tunnels. The length of the tunnels reaches 18 km on the whole. The bypass is designed to allow 140 000 vehicles per day, and it is expected to be completed by 2030

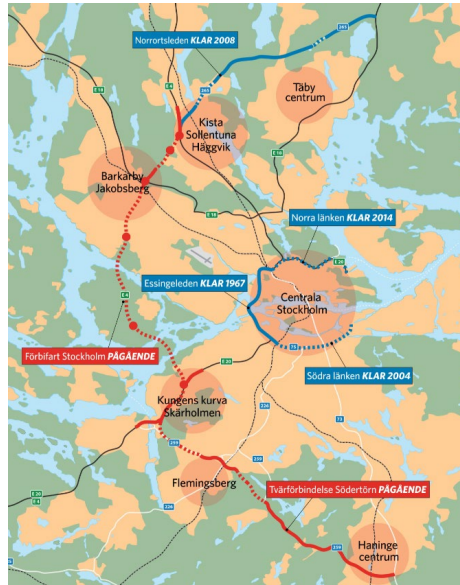


Figure 12 The outer ring road system in Stockholm [19]

The general high quality of the bedrock in Stockholm have facilitated the construction of tunnels and other underground structures in the past few decades. However, several undersea regional fault zones that Bypass project passes through bring challenges and high uncertainties to this project [20]. In addition, several natural and cultural reserves are located around the planned route of this project. This is the reason why the length of tunnel reaches 18km out of 21km, in order to minimize the negative influence of the residential, natural and cultural areas environment.

The deepest point the tunnels reach is located at 65 meters below Lake Mälaren. Two separated parallel tunnel tubes are designed to avoid oncoming traffic. Each tunnel tube consists of 3 lanes.

## 4.2. Geological conditions

Lake Mälaren is the third largest freshwater lake in Sweden. The southern part of the Stockholm Bypass passes through the Lake Mälaren

at three places. The passage under the Lake Mälaren between Sättra and Kungshatt is the first place where the Stockholm Bypass is constructed passing through Lake Mälaren.

The passage under the Lake Mälaren passes through the regional fault zone under the Fiskar fjord. The geological profile of the passage under the Lake Mälaren between Sättra and the island of Kungshatt is illustrated in Figure 13. The bedrock at the location was formed during the Svecofennian orogen [21]. The rock mass under the Lake Mälaren where the subsea passage will be excavated is made up of gneiss of sedimentary origin with intrusions of gneiss-granite and granite. The regional fault zone in the Fiskar fjord can be categorized as a strike-slip fault, which means that the southern part has rotated over the northern part following a dip-slip movement [20].

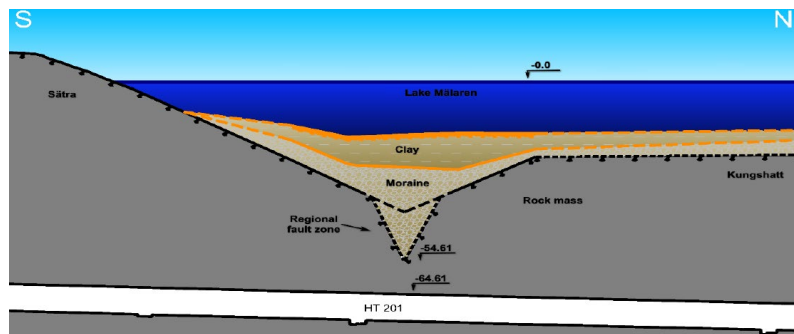


Figure 13 Geological profile of the rock mass between Sättra and Kungshatt [20]

The Gneiss encountered in the passage under the Lake Mälaren is partly heavily fractured, weathered and altered with chlorite, clay and graphite. Besides, the dykes of pegmatites and metabasites are altered in varying degrees cross the rock mass in this area [20]. When the exploratory tunnels were excavated, heavily fractured and weathered rock mass was found concentrated in three major areas. A top view of the passage under the Lake Mälaren and the areas with poor rock qualities is shown in Figure 14.

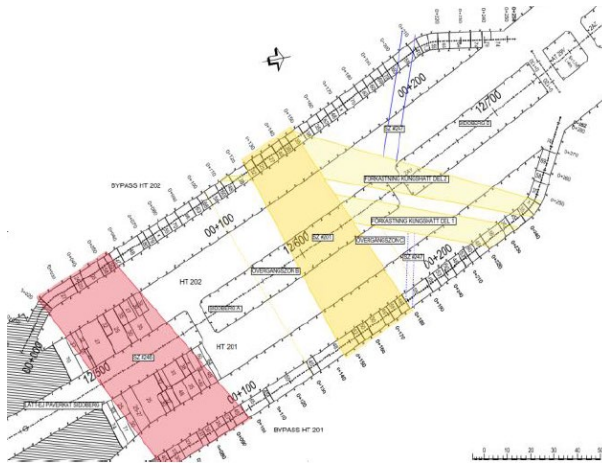


Figure 14 Top view of the subsea passage and areas with poor rock quality [22]

According to the geological investigation, the materials in the fault zones are comprised of cataclasite rock, gouge material and mylonite. Chlorite and graphite are the major components of mineral coatings and infillings in the rock joints. Swelling clay, biotite and calcite only account for a small proportion. In addition, the fault zone is detected to stretch in the E-W direction, crossing the exploratory and main tunnels perpendicularly. The investigation also suggests that the main geological structure has a dip of approximately 70 degrees towards the south. Sub-horizontal and sub-parallel geological structures with respect to the tunnel direction were formed as a result of relative movements between the blocks in the fault zone [20].

The geological mapping shows that subsea passage contains two rock mass qualities. The regional fault zone is approximately 20-30 m in width and has a poor rock mass quality. The estimated  $RMR_{base}$  of the rock mass in the central core of the fault zone is assessed to be between 25 and 40. The rock mass outside the central core of the fault zone has a better quality. In the transition zone of the fault zone, the  $RMR_{base}$  is estimated to be between 40 and 65 [22].

### 4.3. Tunnel geometry and initial support

The subsea passage between Sättra and Kungshatt is made up of two main tunnels (HT201 and HT202) and two exploratory tunnels (BP201 and BP202), as shown in Figure 15. The two main tunnels are approximately 17.8 m in width and 9 m in height. The distance between the two main tunnels is around 12 m. Two exploratory tunnels (also called bypass tunnels) were excavated parallel to the main tunnels. The exploratory tunnels are approximately 8 m high and 6.4 m wide. The distance between the main tunnel and the exploratory tunnel is approximately 13 m.

It should be noted that this master thesis focuses on the exploratory tunnel BP201. Exploratory tunnels were excavated and measured before the construction of the main tunnels started. Therefore, the deformations collected during the excavation of exploratory tunnels were not influenced by the main tunnels.

The exploratory tunnels were excavated first because they can provide more information about the weak zone and help to evaluate the rock mass quality. Besides, after the two sides of the exploratory tunnel are connected, the following subsea passage can be excavated from the end of the exploratory tunnels. In this way, the exploratory tunnels help reduce the total production time of the whole excavation process.

Geological investigations were conducted to estimate the depth of bedrock in the subsea passage. The rock cover where the core of the fault

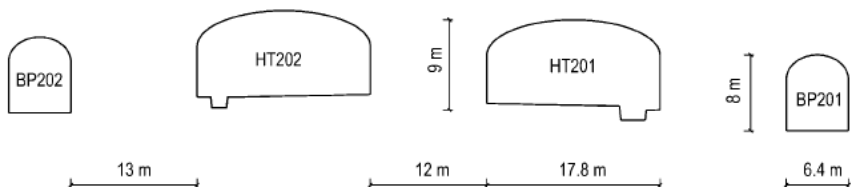


Figure 15 Cross sections of the main and exploratory tunnels in the passage under Lake Mälaren [22]

zone is encountered is around 30-40 m. The thickness of the rock cover at the deepest point is approximately 15 m. In the deepest part of the subsea passage, the rock surface is covered with around 23 m of moraine, 8 m of clay and 16 m of water, as shown in Figure 13.

Due to the poor rock quality of the regional fault zone, combined with a thin rock cover and the existence of Lake Mälaren, the risk of leakage problem must be taken into account during tunnel excavation. Cement grouting together with an observational methodology was adopted in these rock conditions in order to manage the risk of water-induced problem [20].

The grouting of the rock mass in both the exploratory tunnels and the main tunnels was conducted in two rounds in order to reduce the rock mass conductivity. After the first round of grouting was completed, the effectivity was checked by measuring water inflow in several drilled control holes on the front face. The water inflow check after two rounds of grouting determined if a third round was necessary to continue reducing the rock mass conductivity.

Figure 16 and Figure 17 illustrates the grouting procedure of the main tunnels in the perpendicular and parallel directions to the tunnel alignment.

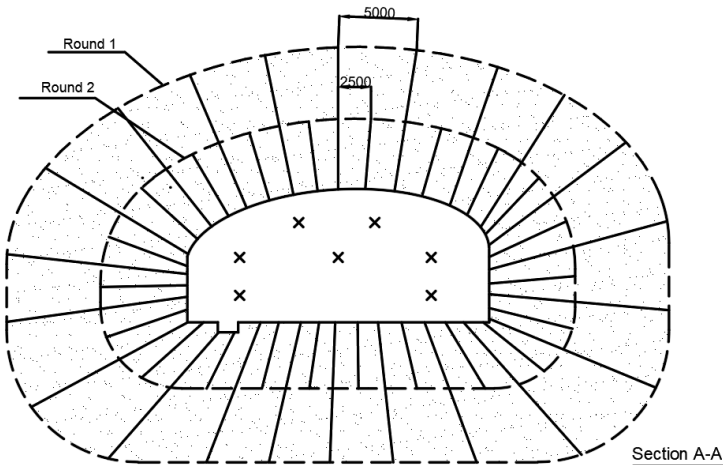


Figure 16 Cross section of the grouting procedure in the main tunnels (perpendicular to the tunnel direction)

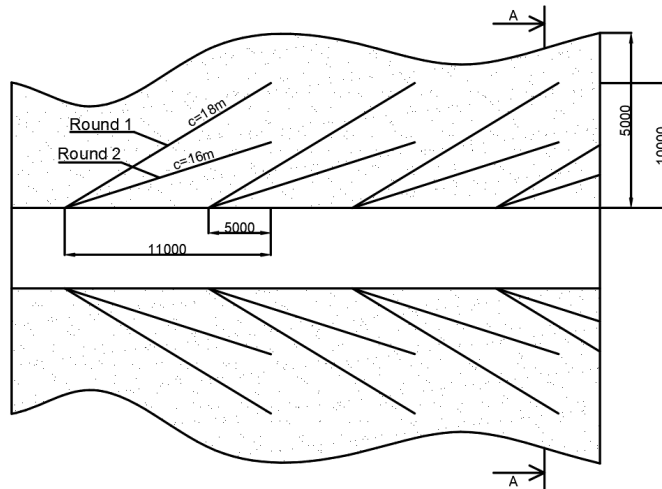


Figure 17 Cross section of the grouting procedure in the main tunnels (parallel to the tunnel direction)

Tunnel instability might happen when the rock mass strength is exceeded. High in-situ stresses in the regional fault zone are one of the main potential causes of rock mass failures under the tunnel excavation. Regarding this, the installation of rock supports is required in early stages in order to stabilize the tunnel crown and the front face [20].

For the exploratory tunnel BP201, the rock bolts have a diameter of 25 mm and are 3 m in length and share the same c/c spacing as the main tunnels, i.e. cc 1 m sideways and cc 2 m along the tunnel. Besides, BP201 has shotcrete of 100 mm thickness. Considering the large tunnel width, the pipe umbrella support system was also applied in order to improve the tunnel stability when the tunnel alignment crosses the regional fault zone. The installation principle of the umbrella pipe support along the tunnel direction is displayed in Figure 18.

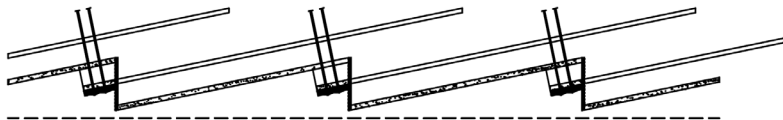


Figure 18 Cross section of the pipe umbrella support in the main tunnel

### 4.4. Deformations in the tunnel

Tunnel deformations were measured with optical convergence in predefined sections in both the main tunnels and the exploratory tunnels. In addition, a combination of extensometers and inclinometers installed in the pipe umbrella were applied to monitor the deformations of two sections along the tunnel direction. The installation positions and the top view of the deformation measurement system is shown in Table 1 and Figure 16.

Table 1 Installation positions of the deformation measurement system

Measurement method	Position			
	BP201	HT201	HT202	BP202
Convergence	0/070	12/513	12/506	0/040
Extensometer	0/068			0/035
Inclinometer		12/515+15/525		

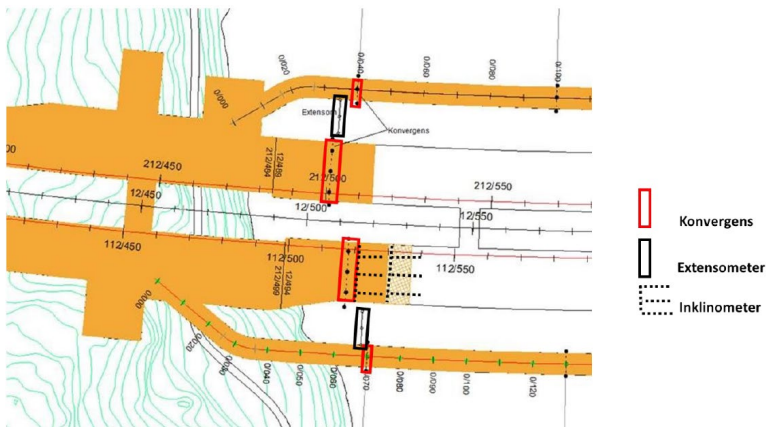


Figure 19 Top view of measurement system in southern part of the subsea passage [22]

The target of the back analysis in this study, the exploratory tunnel BP201, has one measuring prism installed on the tunnel ceiling and two prisms on the tunnel walls, as illustrated in Figure 21. The distance

between two points were measured first. Then, the vertical deformation

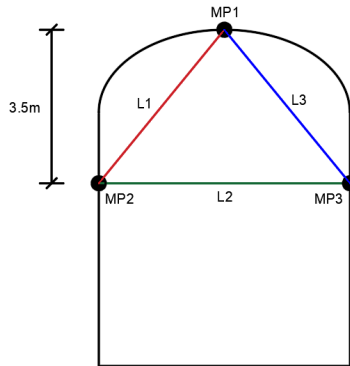


Figure 20 The position of measuring prism in Bypass 201

on the tunnel ceiling and the horizontal deformation on the tunnel walls can be determined by the alteration of relative displacements between measuring prisms under the excavation.

Convergence measurement started on 2018-08-29 with measure prisms installed at the section 0/070. The front face of the top heading is at 0/074 and the front face of the bench is 10 m behind the measurement section, as shown in Figure 21.

## CASE STUDY

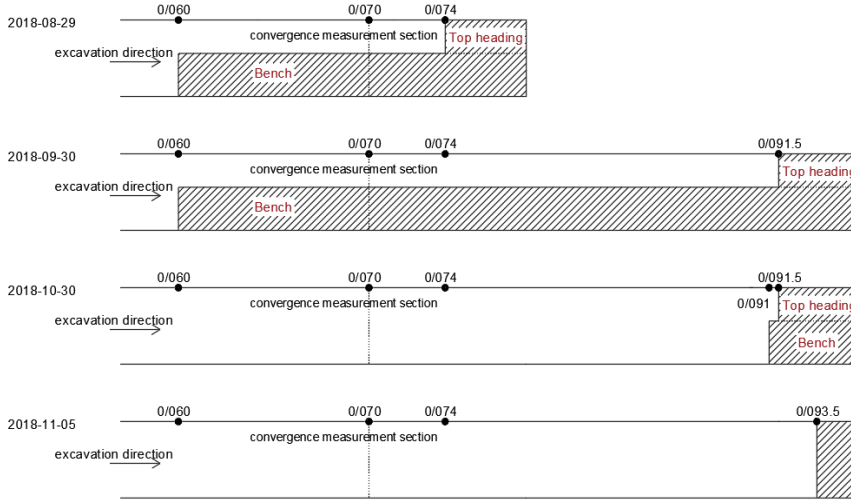


Figure 21 The positions of the tunnel front face on four key time point

As shown in Figure 22, from 2018-08-29 to 2018-09-30, the relative distances among three measurement points in BP201 grew steadily. During this period, five rounds of blasting were conducted in BP201. The top heading of BP201 drifted forwards to 0/091.5, while the bench stayed at the section of 0/060.

In the following 30 days until 2018-10-30, a sharp rise of the deformations in BP201 was observed when the bench was driven to 0/091 while the top heading stood still at the section of 0/091.5. It can be noticed that the extraction of bench rock mass had a significant impact on the relative displacements between L1 and L2.

The top heading and the bench of BP201 started being excavated simultaneously from the section of 0/093.5 since 2018-11-05. The growth of relative displacements among three measurement points started slowing down again because the tunnel front face progressed far away from the measurement section. Finally, the relative displacement L2 was stabilized to 19 mm approximately, and the values of L1 and L3 reached 5 mm and 8 mm respectively. The results of convergence measurement in BP201 at the section of 0/070 is illustrated in Figure 22.

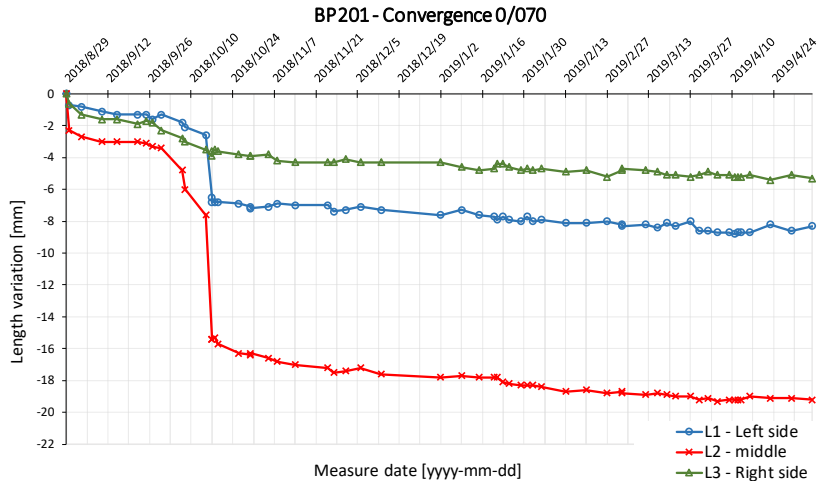


Figure 22 Variation of distance between measuring prisms [22]

The longitudinal variation between measurement points in BP201 were converted into horizontal and vertical deformations so that they can be used in the back analysis. In addition, the initial theoretical deformation, which is assumed to occur prior to the installation of convergence should also be included in the total deformation. The total deformation  $u_{tot}$  on the convergence measurement section can be calculated as equation 4-1, where  $u_m$  is the measured deformation and  $u_i$  is the initial deformation.

$$u_{tot} = u_m + u_i \quad (4 - 1)$$

The tunnel section where measurement was conducted is close to the front face of the tunnel. Elastic deformation as a result of the extraction of rock mass is assumed to begin approximately half a tunnel diameter in front of the tunnel face and to be fully developed two times of the tunnel diameter behind the front face in an unsupported tunnel. It is estimated that around 35% of the total deformation occurred at the tunnel front face. Furthermore, the measurement section behind the front face is assumed to have 40% of the total deformation in BP201 when measurement started. Therefore, the initial deformation can be calculated as:

$$u_i = 0.4 \times u_{tot} \quad (4 - 2)$$

$$u_i = \frac{0.4u_m}{0.6} \quad (4 - 3)$$

Then, the initial horizontal deformation on the tunnel wall,  $u_{i,x}$  and the initial vertical deformation on the tunnel ceiling,  $u_{i,y}$  can be calculated as:

$$u_{i,x} = \frac{0.4u_{m,x}}{0.6} = 1.1mm \quad (4 - 4)$$

$$u_{i,y} = \frac{0.4u_{m,y}}{0.6} = 0.8mm \quad (4 - 5)$$

The total deformation on the wall,  $u_{tot,x}$ , and on the tunnel ceiling,  $u_{tot,y}$ , can be calculated as:

$$u_{tot,x} = u_{i,x} + u_{m,x} = 9.3mm \quad (4 - 6)$$

$$u_{tot,y} = u_{i,y} + u_{m,y} = 2.9mm \quad (4 - 7)$$

In BP201, the horizontal and vertical deformation interpreted from the measurement data can be summarized in Figure 24.

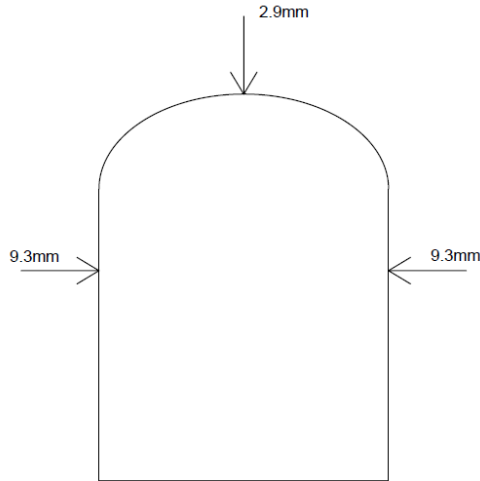


Figure 23 Measured horizontal and vertical total deformations in Bypass 201

## 4.5. Numerical analysis

### 4.5.1. Description of numerical model

In the numerical model of BP201 in Plaxis 2D, the rock mass is simulated with the Mohr-Coulomb model in which the rock mass is regarded as linear elastic and perfectly plastic. A constant average stiffness of the rock mass in the Mohr-Coulomb model can help save the time of computation [15]. For simplicity, rock fractures are not modelled and the influence of flowing water in the rock mass is neglected.

The information about the geological conditions and the rock mass properties in the subsea passage under the Lake Mälaren in this study come from several drill cores performed in this area and two exploratory tunnels. According to the investigations, the Young's modulus ( $E$ ) of the rock mass is estimated to vary from 0.75 GPa to 1.5 GPa and the ratio of horizontal stress over vertical stress ( $k_0$ ) is estimated to be between 0.6 and 1.2 [20]. The properties of the rock mass in the numerical analysis are summarized in Table 2.

Table 2 Rock mass properties in the numerical analysis

<b>Parameter</b>	<b>value</b>
$\varphi [^\circ]$	35
$\gamma [kN/m^3]$	26.5
$\nu [-]$	0.25
$c [MPa]$	0.64
$\sigma_{tm} [MPa]$	0
$\sigma_{cm} [MPa]$	0.6

The material properties of shotcrete in characteristic value are shown in Table 3. The shotcrete is considered as an elastic material and modelled with plate element in the numerical analysis.

Table 3 Material properties of shotcrete

<b>Parameter</b>	<b>Value</b>
$t[mm]$	100/200
$\gamma[kN/m^3]$	23
$E[GPa]$	16
$\nu[-]$	0.25
$f_{cc}[MPa]$	30.5
$f_{ft}[MPa]$	4

The material properties of rock bolts in characteristic value are shown in Table 4. The shotcrete is modelled with embedded beam row elements in Plaxis 2D.

Table 4 Material properties of rock bolts

<b>Parameter</b>	<b>Value</b>
$l[m]$	3
$\phi[mm]$	25
$\gamma[kN/m^3]$	77
$E[GPa]$	200
$f_y[MPa]$	500
$F_y[kN]$	246
$\varepsilon_g[\%]$	5

In order to maintain the stability of the tunnel face and improve the productivity of excavation, the front face is split into top heading (galleri) and bench (pall). The cross section of the numerical model in Plaxis 2D is shown in Figure 24.

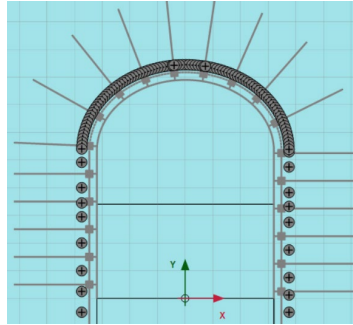


Figure 24 Cross section of BP201 in numerical analysis

Staged construction strategy is applied to simulate the excavation of top heading and bench respectively. The calculation process is divided into four stages. In stage 1, the rock mass of the top heading has been extracted and the tunnel support around the top heading is inactivated. In stage 2, tunnel support of the top heading starts to work. In stage 3, the rock mass of the bench is removed without activating remaining tunnel supports. In the final stage, all the tunnel supports elements are activated. The illustration of the four construction stages are shown in Figure 25.

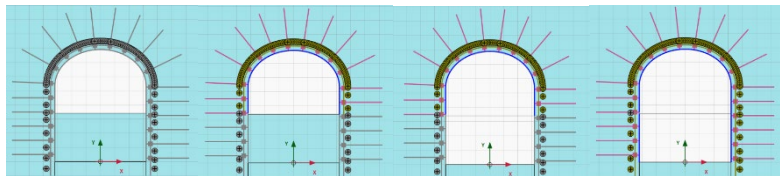


Figure 25 Stage construction (from left to right): stage1, stage2, stage3 and stage4

#### 4.5.2. Estimation of $\sum M_{stage}$

Excavation causes destressing of the rock mass around the opening. The load from increasing rock mass deformation is partly borne by the tunnel support (shotcrete and rock bolts). The rest of the load is redistributed around the excavation opening and then carried by the

surrounding rock mass and tunnel face themselves. As the tunnel face progresses forward, the proportion of the load carried by the tunnel support will increase gradually. When the tunnel face has advanced far away from the section where supports are installed, the tunnel support will carry the full design load.

As mentioned in section 3.1, the proportion of the load imposed on the tunnel support is controlled by the total multiplier  $\sum M_{stage}$  in Plaxis 2D. In order to estimate the value of  $\sum M_{stage}$  in the numerical analysis, an assumption about the percentage of the deformation prior to the installation of supports is made. The percentage of the deformation which accounts for the total deformation in the rock mass is referred as initial deformation rate in this work.

As shown in Table 5, for top heading of BP201, 45% of the total deformation is assumed to happen before top heading is supported. For the bench, the initial deformation is around 55% of the total deformation, which is larger because the rock mass of the bench is removed later than the top heading.

Table 5 Initial deformation of top heading and bench in BP201

Tunnel BP 201	Step	Deformation before step (%)	Deformation after step (%)
Top heading	Top heading is removed	0	45
	Top heading is supported	45	100
Bench	Bench is removed	0	55
	Bench is supported	55	100

The ground reaction curve of each stage can be plotted with Plaxis 2D. Figure 26 describes the ground reaction curve of stage 1, where the top heading has been extracted and tunnel support has not been installed. In this stage, the rock mass is still elastic and the ground reaction curve is

linear. It is assumed that 45% of the total deformation happened in the unsupported top heading. Therefore, the value of  $\sum M_{stage}$  in stage 1 is estimated to be 0.45.

The ground reaction curve of stage 3, the unsupported bench, is shown in Figure 27. After the rock mass of the bench is removed, the rock mass starts to show plastic behavior as the load around the opening increases. The deformation around the bench before installation of support is assumed to be 55%. In this case, the value of  $\sum M_{stage}$  in stage 3 is around 0.61.

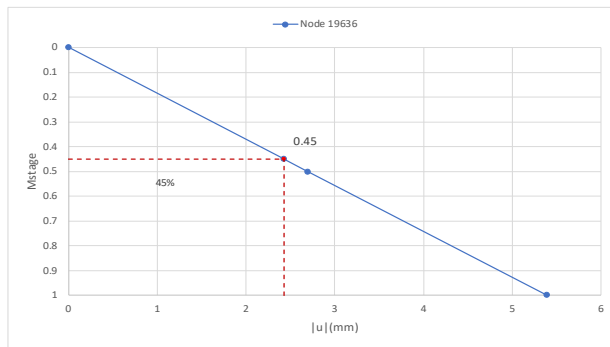


Figure 26 Ground reaction curve of unsupported top heading

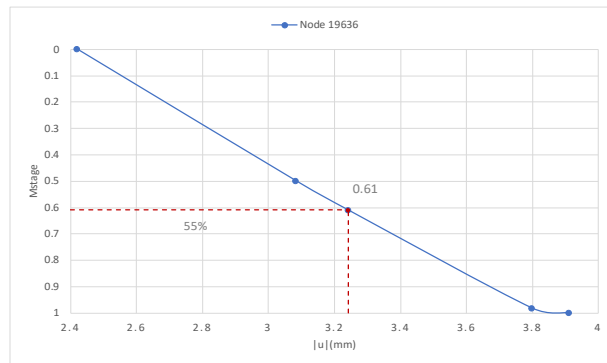


Figure 27 Ground reaction curve of unsupported bench

## 5. Results

### 5.1. Results of numerical analysis

In addition to three convergence measurement points, one central node on the bottom of top heading and one central node on the tunnel floor are also selected in the numerical model, as shown in Figure 29, because the heave of tunnel floor may be a problem under complicated rock mass conditions.

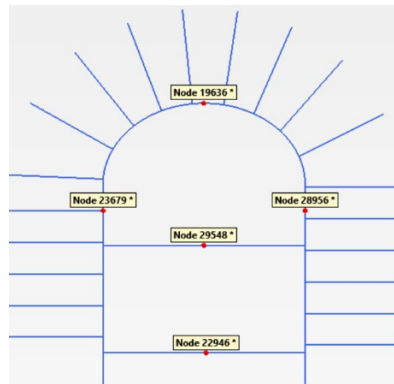


Figure 28 Selected nodes in numerical model

The maximum calculated horizontal deformation  $u_x$ , the maximum vertical deformation  $u_y$  and the maximum total deformation  $|u|$  of five selected nodes are presented in Table 6, using a start value of 0,9 for ( $k_0$ ) and a Young's modulus of 1,125 GPa. The shadings of total deformation in stage 1-4 are shown in Figure 29. The shadings in full scale are attached in Appendix A. It can be observed that larger

displacements of the rock mass occurred on the bottom of the bench and the tunnel floor. The deformation on the tunnel ceiling is relatively small compared to other nodes.

Table 6 Deformations of selected nodes

Deformation Node	$u_x(mm)$	$u_y(mm)$	$ u (mm)$
Node 23679	5.98	-3.02	6.70
Node 28956	5.72	-3.18	6.55
Node 19636	0	-3.33	3.33
Node 29548	0	7.41	7.41
Node 22946	0	8.15	8.15

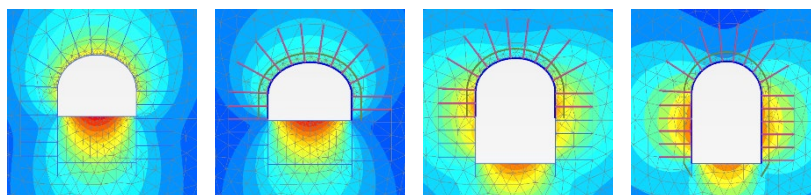


Figure 29 Shadings of deformation of stage 1-4 (from left to right)

## 5.2. Results of back analysis

### 5.2.1. Optimization with the Pattern Search Method

For the pattern search method, the optimization is conducted in a two-dimensional space, where the stress ratio of the horizontal stresses over vertical stresses ( $k_0$ ) is designated as the horizontal axis and the Young's modulus ( $E$ ) as the vertical axis. According to previous geological investigations, the stress ratio of horizontal stresses over vertical stresses ( $k_0$ ) is estimated to vary from 0.6 to 1.2. The range of Young's modulus of the rock mass is assumed to be between 0.75 GPa and 1.5 GPa. The middle point of these two ranges is selected as the starting point of the

back analysis because the middle point has the highest probability to coincide with the optimum point, which can improve the efficiency of the search process. 0.03% is set as the limit value of the error function, which means the search will stop when the value of the error function is lower than 0.03%.

The results of the Pattern Search Method are given in Table 7. 28 rounds of numerical calculations are performed with Plaxis 2D to reach the optimum point. The optimum point highlighted with yellow color in Table 7 shows that the stress ratio is 1.146 and the Young's modulus of the rock mass is 0.957 GPa. The value of the error function at the optimum point is 0.0274%. The search path of the optimization is illustrated in Figure 30.

Table 7 Searching process of pattern search method

Point	Round	k0	E(GPa)	f1(mm)	f2(mm)	f3(mm)	U1(mm)	U2(mm)	U3(mm)	error	
Base X(1)	1	0.9	1.125	5.982	3.328	5.722	9.3	2.9	9.3	0.099029	
	2	0.95	1.125	6.416	3.144	6.153	9.3	2.9	9.3	0.072584	
	3	0.95	1.175	6.164	3.011	5.911	9.3	2.9	9.3	0.082655	
Base X(2)	4	0.95	1.075	6.686	3.288	6.413	9.3	2.9	9.3	0.064424	
	Pattern	5	0.963	1.063	6.878	3.276	6.602	9.3	2.9	9.3	0.056266
Base X(3)	6	1.013	1.063	7.404	3.097	7.133	9.3	2.9	9.3	0.033491	
	7	1.013	1.113	7.036	2.945	6.765	9.3	2.9	9.3	0.044601	
	8	1.013	1.013	7.745	3.252	7.461	9.3	2.9	9.3	0.027264	
Base X(4)	9	1.029	0.998	8.006	3.235	7.719	9.3	2.9	9.3	0.020535	
	10	1.079	0.998	8.542	3.036	8.274	9.3	2.9	9.3	0.007004	
	11	1.079	1.048	8.111	2.881	7.841	9.3	2.9	9.3	0.013667	
Base X(5)	12	1.079	0.948	8.948	3.198	8.678	9.3	2.9	9.3	0.005488	
	13	1.096	0.932	9.27	3.178	8.992	9.3	2.9	9.3	0.003432	
	14	1.146	0.932	9.788	2.958	9.532	9.3	2.9	9.3	0.001259	
Base X(5)	15	1.146	0.982	9.335	2.804	9.086	9.3	2.9	9.3	0.000546	
	16	1.163	0.991	9.433	2.707	9.184	9.3	2.9	9.3	0.001596	
	17	1.213	0.991	9.95	2.502	9.754	9.3	2.9	9.3	0.008701	
Base X(5)	18	1.113	0.991	8.929	2.916	8.671	9.3	2.9	9.3	0.002065	
	19	1.163	1.041	9.021	2.575	8.775	9.3	2.9	9.3	0.005549	
	20	1.163	0.941	9.885	2.853	9.631	9.3	2.9	9.3	0.001829	
Base X(5)	15	1.146	0.982	9.335	2.804	9.086	9.3	2.9	9.3	0.000546	
	Pattern	21	1.159	0.989	9.408	2.732	9.163	9.3	2.9	9.3	0.001236
	Pattern	22	1.156	0.987	9.395	2.75	9.149	9.3	2.9	9.3	0.001014
Base X(5)	Pattern	23	1.153	0.985	9.379	2.766	9.131	9.3	2.9	9.3	0.000846
	Pattern	24	1.149	0.984	9.347	2.786	9.1	9.3	2.9	9.3	0.000678
	explore	25	1.171	0.982	9.594	2.698	9.341	9.3	2.9	9.3	0.001957
26		1.121	0.982	9.083	2.91	8.827	9.3	2.9	9.3	0.001048	
27		1.146	1.007	9.127	2.733	8.877	9.3	2.9	9.3	0.00191	
28		1.146	0.957	9.557	2.878	9.304	9.3	2.9	9.3	0.000274	

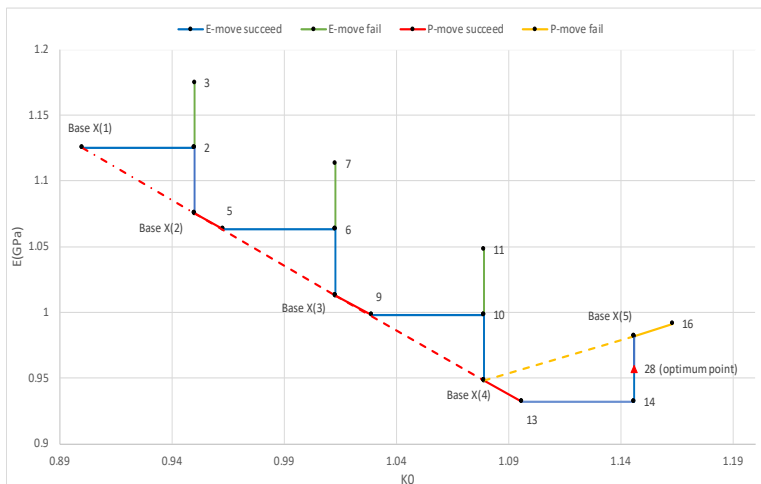


Figure 30 Searching path using the pattern search method

### 5.2.2. Optimization with the Simplex Method

Considering the range of stress ratio (0.6-1.2) and Young's modulus (0.75 GPa-1.5 GPa), The initial simplex is composed of  $X_{(1)}$ (1.2, 1.5),  $X_{(2)}$ (0.9, 0.75) and  $X_{(3)}$ (0.6, 1.125). The optimization stopped when the values of the error function at all the three vertices are no higher than 0.015%. The final simplex is obtained after 17 rounds (34 times) of numerical calculation with Plaxis 2D. The optimum point is located at  $X_{(1)}$  of the final simplex with a value of the error function equal to 0.013%. The stress ratio ( $k_0$ ) at optimum point is 1.136 and the Young's modulus is 0.96GPa. The results of each round of the numerical analysis and the final simplex is shown in Table 8. The search process is illustrated in Figure 31. The detailed transformation of the simplex in each round is given in Appendix B.

RESULTS

Table 8 Searching process using the Simplex Method

	K0	E(GPa)	f1(mm)	f2(mm)	f3(mm)	U1(mm)	U2(mm)	U3(mm)	error
Round1									
X1	1.200	1.500	6.591	1.663	6.356	9.3	2.9	9.3	0.12234
X2	0.900	0.750	8.785	5.023	8.445	9.3	2.9	9.3	0.18248
X3	0.600	1.125	3.371	4.424	3.199	9.3	2.9	9.3	0.37099
middle point of X1X2	1.050	1.125							
X4	1.500	1.125	11.332	1.104	11.097	9.3	2.9	9.3	0.15621
Round2									
X1	1.200	1.500	6.591	1.663	6.356	9.3	2.9	9.3	0.12234
X2	1.500	1.125	11.332	1.104	11.097	9.3	2.9	9.3	0.15621
X3	0.900	0.750	8.785	5.023	8.445	9.3	2.9	9.3	0.18248
middle point of X1X2	1.350	1.313							
X4	1.800	1.875	9.034	0.089	8.943	9.3	2.9	9.3	0.31395
X6	1.125	1.031	8.728	2.753	8.481	9.3	2.9	9.3	0.00470
Round3									
X1	1.125	1.031	8.728	2.753	8.481	9.3	2.9	9.3	0.00470
X2	1.200	1.500	6.591	1.663	6.356	9.3	2.9	9.3	0.12234
X3	1.500	1.125	11.332	1.104	11.097	9.3	2.9	9.3	0.15621
middle point of X1X2	1.163	1.266							
X4	0.825	1.406	4.341	2.892	4.134	9.3	2.9	9.3	0.19763
X6	1.331	1.195	9.433	1.665	9.432	9.3	2.9	9.3	0.06059
Round4									
X1	1.125	1.031	8.728	2.753	8.481	9.3	2.9	9.3	0.00470
X2	1.331	1.195	9.433	1.665	9.432	9.3	2.9	9.3	0.06059
X3	1.200	1.500	6.591	1.663	6.356	9.3	2.9	9.3	0.12234
middle point of X1X2	1.228	1.113							
X4	1.256	0.727	13.679	3.209	13.424	9.3	2.9	9.3	0.14323
X6	1.214	1.307	7.593	1.862	7.336	9.3	2.9	9.3	0.06880
Round5									
X1	1.125	1.031	8.728	2.753	8.481	9.3	2.9	9.3	0.00470
X2	1.331	1.195	9.433	1.665	9.432	9.3	2.9	9.3	0.06059
X3	1.214	1.307	7.593	1.862	7.336	9.3	2.9	9.3	0.06880
middle point of X1X2	1.228	1.113							
X4	1.242	0.920	10.923	2.567	10.700	9.3	2.9	9.3	0.02210
Round6									
X1	1.125	1.031	8.728	2.753	8.481	9.3	2.9	9.3	0.00470
X2	1.242	0.920	10.923	2.567	10.700	9.3	2.9	9.3	0.02210
X3	1.331	1.195	9.433	1.665	9.432	9.3	2.9	9.3	0.06059
middle point of X1X2	1.184	0.976							
X4	1.036	0.756	10.412	4.258	10.115	9.3	2.9	9.3	0.08042
X6	1.257	1.085	9.576	2.118	9.492	9.3	2.9	9.3	0.02467
Round7									
X1	1.125	1.031	8.728	2.753	8.481	9.3	2.9	9.3	0.00470
X2	1.242	0.920	10.923	2.567	10.700	9.3	2.9	9.3	0.02210
X3	1.257	1.085	9.576	2.118	9.492	9.3	2.9	9.3	0.02467
middle point of X1X2	1.184	0.976							
X4	1.110	0.866	10.062	3.359	9.783	9.3	2.9	9.3	0.01149
Round8									
X1	1.125	1.031	8.728	2.753	8.481	9.3	2.9	9.3	0.00470
X2	1.110	0.866	10.062	3.359	9.783	9.3	2.9	9.3	0.01149
X3	1.242	0.920	10.923	2.567	10.700	9.3	2.9	9.3	0.02210
middle point of X1X2	1.117	0.948							
X4	0.993	0.977	7.804	3.455	7.509	9.3	2.9	9.3	0.03320
X6	1.180	0.934	10.135	2.802	9.883	9.3	2.9	9.3	0.00438
Round9									
X1	1.180	0.934	10.135	2.802	9.883	9.3	2.9	9.3	0.00438
X2	1.125	1.031	8.728	2.753	8.481	9.3	2.9	9.3	0.00470
X3	1.110	0.866	10.062	3.359	9.783	9.3	2.9	9.3	0.01149
middle point of X1X2	1.152	0.983							
X4	1.195	1.100	8.891	2.321	8.733	9.3	2.9	9.3	0.01517
X6	1.131	0.924	9.707	3.051	9.445	9.3	2.9	9.3	0.00162

Round10									
X1	1.131	0.924	9.707	3.051	9.445	9.3	2.9	9.3	0.00162
X2	1.180	0.934	10.135	2.802	9.883	9.3	2.9	9.3	0.00438
X3	1.125	1.031	8.728	2.753	8.481	9.3	2.9	9.3	0.00470
middle point of X1X2	1.155	0.929							
X4	1.186	0.827	11.369	3.145	11.124	9.3	2.9	9.3	0.03170
X6	1.140	0.980	9.289	2.837	9.040	9.3	2.9	9.3	0.00042
Round11									
X1	1.140	0.980	9.289	2.837	9.040	9.3	2.9	9.3	0.00042
X2	1.131	0.924	9.707	3.051	9.445	9.3	2.9	9.3	0.00162
X3	1.180	0.934	10.135	2.802	9.883	9.3	2.9	9.3	0.00438
middle point of X1X2	1.136	0.952							
X4	1.092	0.970	8.898	3.069	8.627	9.3	2.9	9.3	0.00350
X6	1.114	0.961	9.192	3.004	8.931	9.3	2.9	9.3	0.00100
Round12									
X1	1.140	0.980	9.289	2.837	9.040	9.3	2.9	9.3	0.00042
X2	1.114	0.961	9.192	3.004	8.931	9.3	2.9	9.3	0.00100
X3	1.131	0.924	9.707	3.051	9.445	9.3	2.9	9.3	0.00162
middle point of X1X2	1.127	0.971							
X4	1.123	1.017	8.817	2.801	8.565	9.3	2.9	9.3	0.00337
X6	1.129	0.947	9.471	2.985	9.212	9.3	2.9	9.3	0.00043
Round13									
X1	1.140	0.980	9.289	2.837	9.040	9.3	2.9	9.3	0.00042
X2	1.129	0.947	9.471	2.985	9.212	9.3	2.9	9.3	0.00043
X3	1.114	0.961	9.192	3.004	8.931	9.3	2.9	9.3	0.00100
middle point of X1X2	1.135	0.964							
X4	1.156	0.966	9.577	2.810	9.331	9.3	2.9	9.3	0.00062
X6	1.145	0.965	9.474	2.859	9.222	9.3	2.9	9.3	0.00021
Round14									
X1	1.145	0.965	9.474	2.859	9.222	9.3	2.9	9.3	0.00021
X2	1.140	0.980	9.289	2.837	9.040	9.3	2.9	9.3	0.00042
X3	1.129	0.947	9.471	2.985	9.212	9.3	2.9	9.3	0.00043
middle point of X1X2	1.143	0.973							
X4	1.156	0.998	9.300	2.719	9.056	9.3	2.9	9.3	0.00153
X6	1.136	0.960	9.427	2.913	9.171	9.3	2.9	9.3	0.00013
Round15									
X1	1.136	0.960	9.427	2.913	9.171	9.3	2.9	9.3	0.00013
X2	1.145	0.965	9.474	2.859	9.222	9.3	2.9	9.3	0.00021
X3	1.140	0.980	9.289	2.837	9.040	9.3	2.9	9.3	0.00042
middle point of X1X2	1.140	0.963							
X4	1.141	0.945	9.614	2.938	9.359	9.3	2.9	9.3	0.00045
X6	1.140	0.971	9.368	2.864	9.118	9.3	2.9	9.3	0.00020
Round16									
X1	1.136	0.960	9.427	2.913	9.171	9.3	2.9	9.3	0.00013
X2	1.140	0.971	9.368	2.864	9.118	9.3	2.9	9.3	0.00020
X3	1.145	0.965	9.474	2.859	9.222	9.3	2.9	9.3	0.00021
middle point of X1X2	1.138	0.966							
X4	1.131	0.966	9.323	2.915	9.067	9.3	2.9	9.3	0.00022
X6	1.142	0.965	9.441	2.873	9.191	9.3	2.9	9.3	0.00015
Round17									
X1	1.136	0.960	9.427	2.913	9.171	9.3	2.9	9.3	0.00013
X2	1.142	0.965	9.441	2.873	9.191	9.3	2.9	9.3	0.00015
X3	1.140	0.971	9.368	2.864	9.118	9.3	2.9	9.3	0.00020
middle point of X1X2	1.139	0.963							
X4	1.137	0.954	9.491	2.927	9.235	9.3	2.9	9.3	0.00019
X6	1.138	0.958	9.465	2.910	9.211	9.3	2.9	9.3	0.00014
The final simplex									
X1	1.136	0.960	9.427	2.913	9.171	9.3	2.9	9.3	0.00013
X2	1.138	0.958	9.465	2.910	9.211	9.3	2.9	9.3	0.00014
X3	1.142	0.965	9.441	2.873	9.191	9.3	2.9	9.3	0.00015

# RESULTS

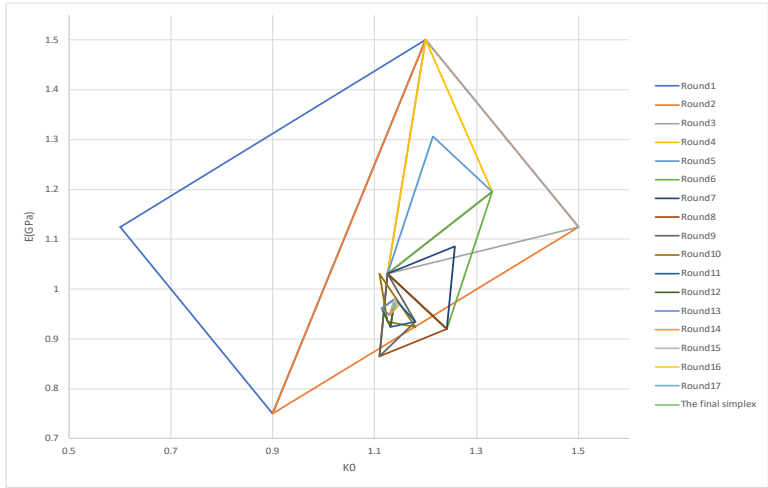


Figure 31 Searching progress using the Simplex Method

## 6. Discussion

### 6.1. Comparison between two optimization algorithms

Both the Pattern Search Method and the Simplex Method belong to classical optimization algorithms. Compared to methods which require the calculation of derivatives, the Pattern Search Method and the Simplex method always take more calculation to converge and suffer from a lower efficiency. However, the difficulty to obtain derivative or the absence of derivative is a common problem in a highly nonlinear error function. In this case, without the bother of calculating derivative, both the Pattern Search Method and the Simplex Method are easy to perform manually and program in the computer. For the problem which only has limited unknown parameters, these two methods can always lead to a satisfactory result.

In this study, with two unknown parameters (stress ratio and Young's modulus), optimization with two methods is performed in a two-dimensional space. Considering the starting point (0.9, 1.125), the Pattern Search Method takes 28 rounds of numerical calculations to reach the optimum point, with the error function equal to 0.000274. For the Simplex Method, the initial simplex is made up of (1.2, 1.5), (0.9, 0.75) and (0.6, 1.125), and it takes 34 rounds of numerical calculation to converge. However, it is unreasonable to conclude that the Pattern Search Method is more effective than the Simplex Method in this study, because the number of rounds highly depends on the starting point of the optimization. It can be observed in section 6.3 that the second optimization with the Pattern Search Method, after the starting point is changed to (0.6, 0.75), spends 38 rounds of numerical calculations to

converge, which is even more than the number of rounds the Simplex Method spends.

One advantage of the Simplex Method in this study is its simplicity. In the Simplex Method, the value of the error function at each vertex is compared and then transferred into a new simplex regardless of the dimension of the simplex. It means that optimization follows the same normalized steps even though the simplex is quite close to the optimum point. However, for the Pattern Search Method, when the search path is close to the optimum point, the step size of the exploratory move  $\delta$  is sometimes so large that the exploratory move will “miss” the optimum point and further lead to the failure of the pattern move. In this situation, the search path has to go back to the last base point, and then the step size has to be adjusted frequently so that the search path can reach the optimum point. This is the reason why the amount of numerical analysis rises dramatically when the search path is close to the optimum point.

Table 9 shows that optimizations with the Pattern Search Method and the Simplex Method relatively close to the optimum point. Both methods can converge and meet the requirement of the error function. As mentioned in section 6.3, local optimum points might be a problem of back analysis with classical optimization algorithms. The similarity of the results from the two optimization methods demonstrates the correctness of each other and also reduces the possibility of a local optimum.

Table 9 Comparison of results using the two optimization algorithms

Optimization algorithm	Optimum point		Error function
	$K_0$	$E$ (GPa)	
Pattern Search Method	1.146	0.957	0.00027
Simplex Method	1.136	0.960	0.00013

## 6.2. Influence of $\sum M_{stage}$

The initial deformation prior to the installation of support influences the estimation of  $\sum M_{stage}$ , and further has impacts on the numerical analysis results and the back analysis results. In order to study the sensitivity of the back analysis to the alteration of  $\sum M_{stage}$ , the percentage of initial deformation accounting for the total deformation is assumed to increase 10% and decrease 10% respectively, as shown in Table 10.

Table 10 Alteration of initial deformation in sensitivity analysis

	Initial percentage	Increased percentage (10%)	Decreased percentage (10%)
Top heading	45%	55%	35%
Bench	55%	65%	45%

Under different assumptions of initial deformation percentage, the ground reaction curves of un-supported top heading and bench can be plotted to estimate the value of  $\sum M_{stage}$ , as shown in Figure 33, Figure 34, Figure 35 and Figure 36. The values of  $\sum M_{stage}$  are also summarized in Table 11.

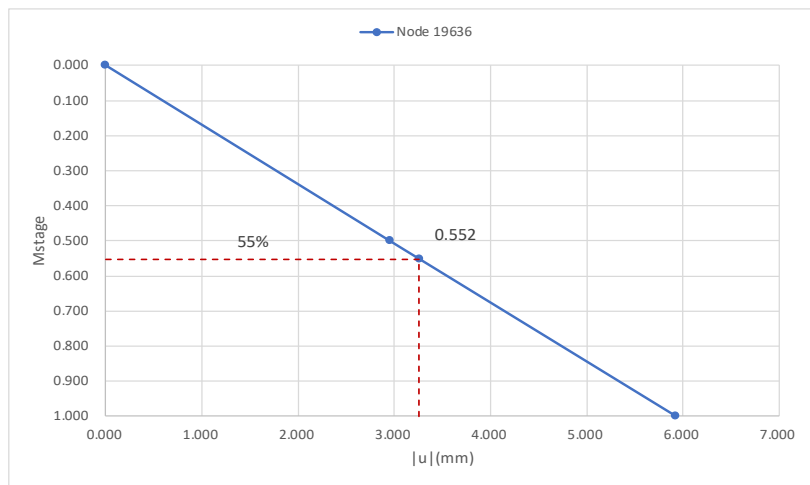


Figure 32  $\sum M_{stage}$  of top heading with initial deformation accounting for 55%

DISCUSSION

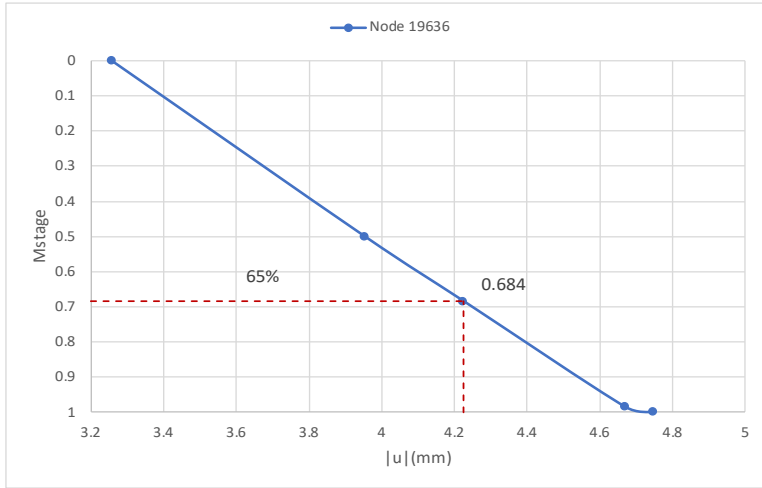


Figure 33  $\Sigma Mstage$  of bench with initial deformation accounting for 65%

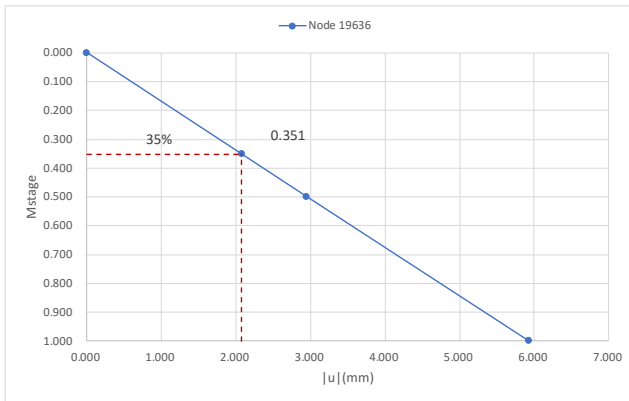


Figure 34  $\Sigma Mstage$  of top heading with initial deformation accounting for 35%

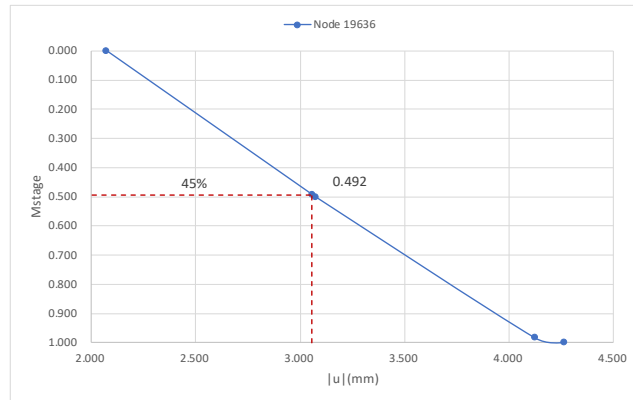


Figure 35  $\Sigma Mstage$  of bench with initial deformation accounting for 45%

Table 11 Values of  $\Sigma Stage$  after alteration of initial deformation

	Initial percentage	Increased percentage (10%)	Decreased percentage (10%)
Top heading	0.450	0.552	0.351
Bench	0.610	0.684	0.492

The simplex Method is applied in this sensitivity analysis, because compared to the Pattern Search Method, the process of the Simplex Method is more normalized. Even though the value of  $\Sigma Mstage$  is changed in the numerical model, the optimization process starts from the same initial simplex and follows the normalized rule mentioned in section 3.3.2. However, in the Pattern Search Method, when the search path is approaching the optimum point, a large amount of exploratory moves are required. In addition, the frequent alteration of the step size and basement points around the optimum point also reduces the accuracy and efficiency of the optimization process. Therefore, the Simplex Method is preferred in the sensitivity analysis.

The final simplex under three different assumptions are plotted in Figure 36 and the coordinates of the vertices including the optimum point are summarized in Table 12. The results and the search paths in the sensitivity analysis are given in Appendix C.

Table 12 shows that the change of  $\sum Mstage$  has a relatively little influence on the results of the back analysis. All three optimum points are close to each other and can fulfill the requirement of the error function. In summary, lower initial deformation rates leads to slightly smaller Young's modulus and slightly smaller stress ratio in the back analysis. Lower initial deformation implies that less load is carried by the rock mass around the opening, and higher proportion of the load will be borne by the tunnel support system. In this case, the Young's modulus of the rock mass has to be lower in order to obtain lower stiffness so that more load can be taken by the tunnel support.

From the perspective of stress ratio, large deformation and some other rock mass behaviors are always caused by the difference between horizontal and vertical in-situ stresses. In this sensitivity analysis, we assume that smaller deformations occurs prior to the installation of support, which will definitely make the back analysis obtain a smaller stress ratio. In other words, the rock mass has a higher quality. Therefore, the results from the sensitivity analysis are reasonable.

According to Figure 32, 34, 35 and 36 in the most part of the ground reaction curve, the rock mass is elastic and has an almost linear behavior. Therefore, the increasement and decrement of initial deformation rate lead to a linear change of the  $\sum Mstage$  value. Furthermore, it can be observed from Table 12 that the stress ratio and Young's modulus also have an approximate linear variation.

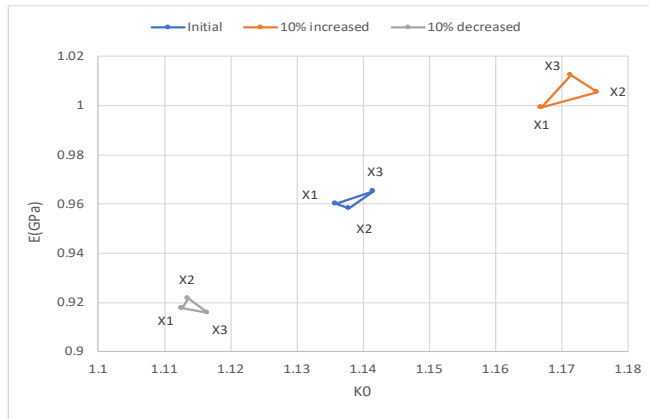


Figure 36 Final simplex under different assumptions of initial deformation

Table 12 Coordinate of final simplex under different assumptions of initial deformation

	Vertex	$K_0$	$E$ (GPa)	Error	
Initial	$X_1$	1.136	0.960	0.00013	Optimum
	$X_2$	1.138	0.958	0.00014	
	$X_3$	1.142	0.965	0.00015	
10% increased	$X_1$	1.167	0.999	0.00009	Optimum
	$X_2$	1.175	1.006	0.00011	
	$X_3$	1.171	1.012	0.00014	
10% decreased	$X_1$	1.113	0.918	0.00016	Optimum
	$X_2$	1.114	0.922	0.00017	
	$X_3$	1.117	0.916	0.00018	

### 6.3. Influence of starting point

As mentioned in section 1.4, back analysis with the Pattern Search Method is a local search in a limited parameter space, which means that the optimum obtained from the Pattern Search Method is perhaps not the optimum in the entire parameter space. In this study, the back analysis is only performed with respect to two geological parameters (stress ratio and Young's modulus), and the degree of nonlinearity is relatively low. Therefore, the possibility that the pattern search ends up with a local

optimum is not such a concerning problem. In order to reduce the suspicion of a local optimum, another optimization with the Pattern Search Method is carried out from the starting point (0.6,0.75). For simplicity, the Pattern Search Method is applied in this verification because only one starting point is required compared to three starting points in the Simplex Method. The search path is shown in Figure 37.

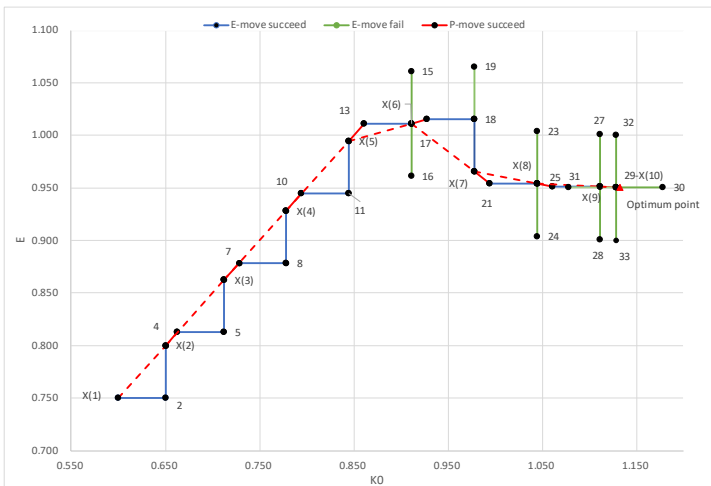


Figure 37 Search path starting from (0.6,0.75)

The search paths using the Pattern Search Method starting from different points are compared in Figure 38, and the results of the two optimizations are summarized in Table 13. Table 13 shows that the optimum points of two back analysis are (1.146, 0.957) and (1.132, 0.950), respectively. Both results meet the requirement of the error function and the optimum points are quite close to each other. The second back analysis improves the possibility that the global optimum point is obtained.

It should be noticed that 38 rounds of numerical analysis are run in the second optimization, which is much larger than the number in the first optimization (28 rounds). Therefore, it is preferable to have a proper estimation on the range of unknown parameters before the back analysis

is performed, which can save the time of optimization and reduce the risk of local optimum. Besides, the pattern search is preferable to start from the middle point of the range, which can improve the efficiency of the Pattern Search Method.

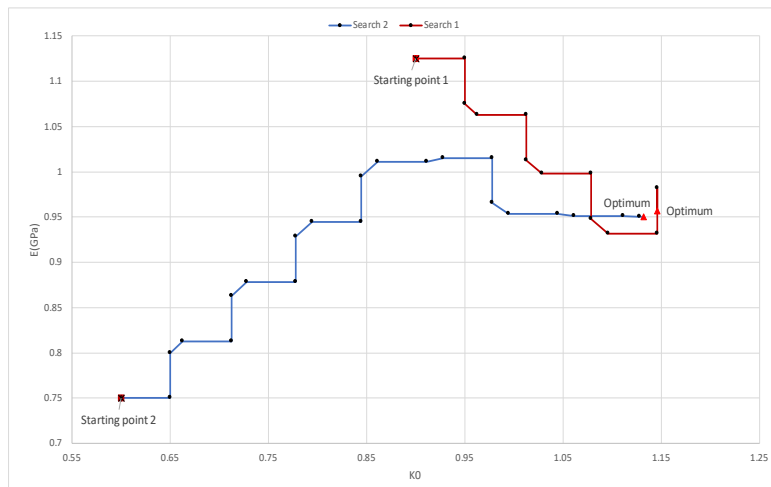


Figure 38 Comparison of two optimizations

Table 13 Results of two optimizations

	Starting point	Optimum	Number of rounds	$K_0$	$E(GPa)$	Minimum error
Search 1	(0.9, 1.125)	(1.146, 0.957)	28	1.146	0.957	0.000274
Search 2	(0.6, 0.75)	(1.132, 0.950)	38	1.132	0.950	0.000287

## 7. Conclusions

In this thesis, pattern search method and simplex method are applied to back analyze the stress ratio and Young's modulus in the Bypass 201 of the passage through the regional fault zone under the Lake Mälaren in the Stockholm Bypass Project. It can be concluded that the stress ratio of horizontal stresses over vertical stresses is around 1.14 and the Young's modulus of the rock mass is around 0.96 GPa. These results can be applied as reference in the prediction of tunnel deformations and the design of geological projects in nearby domains.

Concerning the optimization algorithms, the Simplex Method is preferable because of the higher simplicity and precision compared to the Pattern Search Method. Another conclusion drawn from the sensitivity analysis is that the change of initial deformations has a relatively small influence on the results of the back analysis. Besides, the efficiency of two optimization algorithms to a large extent depends on the choice of starting point. A good choice of the starting point can save computation time and lead to better results.

Generally, back analysis techniques tend to have a higher reliability in ideal good rock mass conditions. The existence of ground water, fault zones and other complex geological conditions has negative impacts on the results of back analysis. It is worth noting that the passage under the Lake Mälaren is excavated through the regional fault zone and has high uncertainties in the rock mass. Thus, it is difficult to conclude that the results in this study are reliable in the entire field of the project. It is recommended to perform several field tests in order to verify the results of the back analysis. Another possible reason for the reliability problem is that the deformation monitoring system is only applied in one cross

section of BP201. The limited number of deformation data also has an influence on the reliability of the back analysis.

In order to improve the quality of the back analysis, it is worth to measure tunnel deformations in more cross sections. In that case, a 3D numerical model can be applied to be able to perform a careful consideration of the deformations at different points along the tunnel.

The correctness of the numerical model also influences the precision of the back analysis. In this study, displacement-based back analysis only takes tunnel deformation into consideration. In addition to displacement, stresses in the rock mass are another important output of the numerical analysis. Including stresses into the error function can make the numerical fit better to the reality and lead to more reasonable results of the back analysis. However, that requires that the stresses in the rock mass is measured, which is not an easy task.

## 8. References

- [1] R. Singh, A. Kainthola, and T. Singh, "Estimation of elastic constant of rocks using an ANFIS approach," *Applied Soft Computing*, vol. 12, no. 1, pp. 40-45, 2012.
- [2] H. Zhao, F. Ma, J. Xu, and J. Guo, "In situ stress field inversion and its application in mining-induced rock mass movement," *International journal of rock mechanics and mining sciences (Oxford, England : 1997)*, vol. 53, pp. 120-128, 2012, doi: 10.1016/j.ijrmms.2012.05.005.
- [3] A. Palmstrom and H. Stille, "Ground behaviour and rock engineering tools for underground excavations," *Tunnelling and underground space technology*, vol. 22, no. 4, pp. 363-376, 2007, doi: 10.1016/j.tust.2006.03.006.
- [4] E. Hoek and M. S. Diederichs, "Empirical estimation of rock mass modulus," *International Journal of Rock Mechanics and Mining Sciences*, vol. 43, no. 2, pp. 203-215, 2006, doi: 10.1016/j.ijrmms.2005.06.005.
- [5] D. M. Ivars, F. Johansson, R. Ghazal, A. Sánchez Juncal, and R. Batres Estrada, "A case study of the Odenplan station in the Stockholm City Link project-Analysis of in situ stresses and observed ground behaviour," ed, 2016.
- [6] T. Miranda, D. Dias, S. Eclaircy-Caudron, A. Gomes Correia, and L. Costa, "Back analysis of geomechanical parameters by optimisation of a 3D model of an underground structure," *Tunnelling and Underground Space Technology incorporating Trenchless Technology Research*, vol. 26, no. 6, pp. 659-673, 2011, doi: 10.1016/j.tust.2011.05.010.
- [7] A. Cividini, L. Jurina, and G. Gioda, "Some aspects of 'characterization' problems in geomechanics," *International Journal of Rock Mechanics and Mining Sciences and Geomechanics Abstracts*, vol. 18, no. 6, pp. 487-503, 1981, doi: 10.1016/0148-9062(81)90513-1.
- [8] S. Sakurai and K. Takeuchi, "Back analysis of measured displacements of tunnels," *Rock Mechanics and Rock Engineering*, vol. 16, no. 3, pp. 173-180, 1983, doi: 10.1007/BF01033278.
- [9] P. Oreste, "Back-analysis techniques for the improvement of the understanding of rock in underground constructions," *Tunnelling*

- and Underground Space Technology incorporating Trenchless Technology Research*, vol. 20, no. 1, pp. 7-21, 2005, doi: 10.1016/j.tust.2004.04.002.
- [10] M. Yazdani, M. Sharifzadeh, K. Kamrani, and M. Ghorbani, "Displacement-based numerical back analysis for estimation of rock mass parameters in Siah Bisheh powerhouse cavern using continuum and discontinuum approach," *Tunnelling and Underground Space Technology incorporating Trenchless Technology Research*, vol. 28, no. C, pp. 41-48, 2012, doi: 10.1016/j.tust.2011.09.002.
- [11] Y. S. Jeon and H. S. Yang, "Development of a back analysis algorithm using flac," *International Journal of Rock Mechanics and Mining Sciences*, vol. 41, no. 3, pp. 441-442, 2004, doi: 10.1016/j.ijrmms.2003.12.085.
- [12] X.-T. Feng, Z. Zhang, and Q. Sheng, "Estimating mechanical rock mass parameters relating to the Three Gorges Project permanent shiplock using an intelligent displacement back analysis method," *International Journal of Rock Mechanics and Mining Sciences*, vol. 37, no. 7, pp. 1039-1054, 2000, doi: 10.1016/S1365-1609(00)00035-6.
- [13] L. Costa, "A parameter-less evolution strategy for global optimization," in *IEEE congress on evolutionary computation (CEC)*, 2005.
- [14] S. S. Vardakos, M. S. Gutierrez, and N. R. Barton, "Back-analysis of Shimizu Tunnel No. 3 by distinct element modeling," *Tunnelling and Underground Space Technology incorporating Trenchless Technology Research*, vol. 22, no. 4, pp. 401-413, 2007, doi: 10.1016/j.tust.2006.10.001.
- [15] R. Brinkgreve *et al.*, "PLAXIS 2D Reference manual," *Delft University of Technology and PLAXIS bv The Netherlands*, 2011.
- [16] N. Moreira *et al.*, "Back analysis of geomechanical parameters in underground works using an Evolution Strategy algorithm," *Tunnelling and Underground Space Technology incorporating Trenchless Technology Research*, vol. 33, no. C, pp. 143-158, 2013, doi: 10.1016/j.tust.2012.08.011.
- [17] R. Hooke and T. Jeeves, "`` Direct Search" Solution of Numerical and Statistical Problems," *Journal of the ACM (JACM)*, vol. 8, no. 2, pp. 212-229, 1961, doi: 10.1145/321062.321069.
- [18] I. Grešovnik, "Simplex algorithms for nonlinear constraint optimization problems," revision, 2007.
- [19] "Why is a bypass needed? - E4 The Stockholm bypass Project." <https://www.trafikverket.se/en/startpage/projects/Road-construction-projects/the-stockholm-bypass/Why-is-a-bypass-needed---E4-The-Stockholm-bypass-Project/> (accessed).
- [20] B. Stille, F. Johansson, F. Ríos Bayona, R. Batres Estrada, and M. Roslin, "Stockholm bypass project – passage under the Lake Mälaren," ed, 2019, pp. 1569-1578.

## REFERENCES

- [21] G. Gaál and R. Gorbatshev, "An Outline of the precambrian evolution of the baltic shield," *Precambrian Research*, vol. 35, no. C, pp. 15-52, 1987, doi: 10.1016/0301-9268(87)90044-1.
- [22] B. Stille, F. Ríos-Bayona, F. Johansson, L. Sjölund, R. Batres-Estrada, and M. Roslin, "Strategy for the permanent technical solution under the Lake Mälaren in the Stockholm Bypass Project."

# Appendix A

## The shadings of total deformation from Plaxis 2D

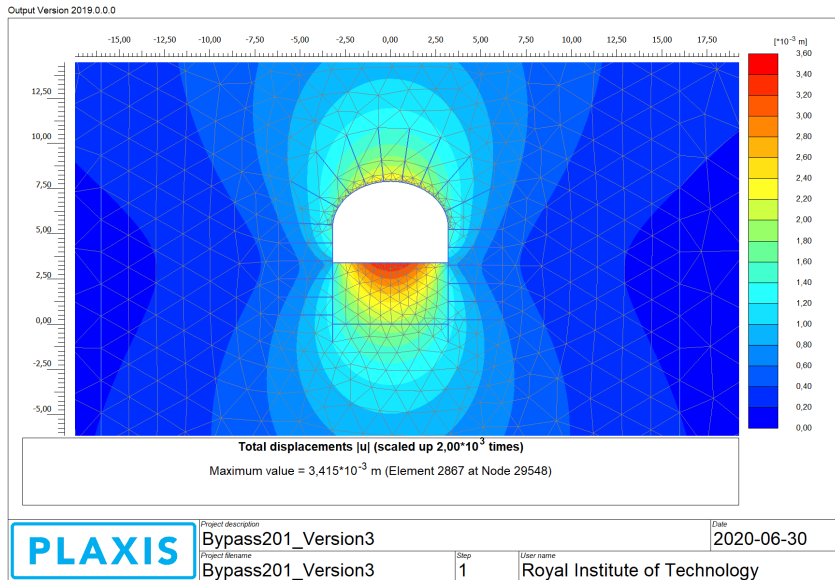


Figure 39 Shading of total deformation in stage 1

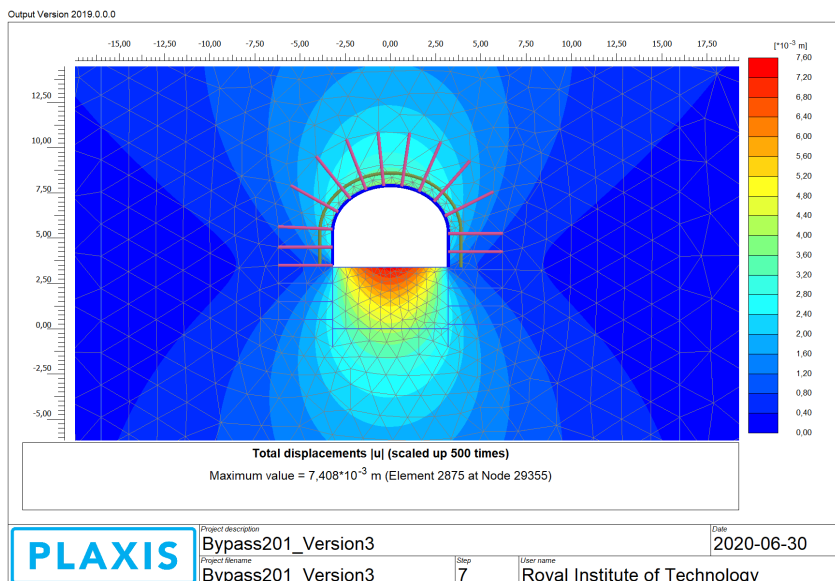


Figure 40 Shading of total deformation in stage 2

APPENDIX A

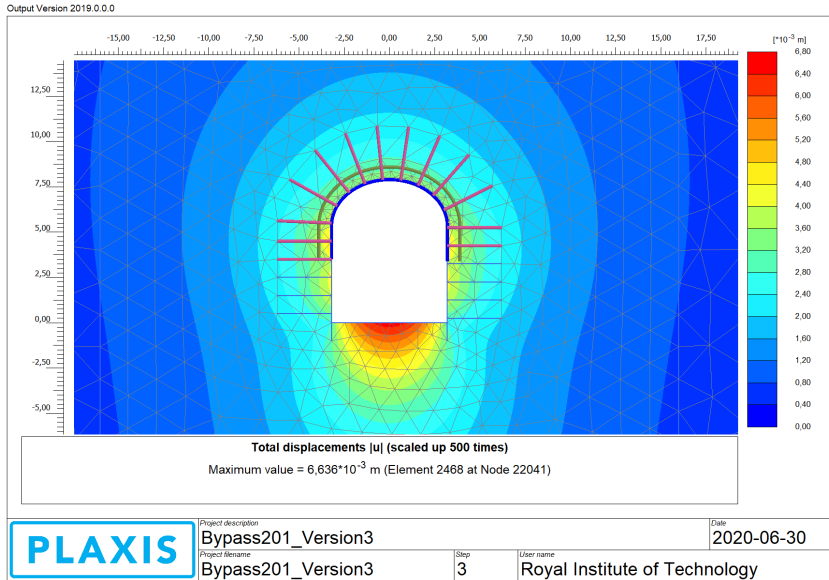


Figure 41 Shading of total deformation in stage 3

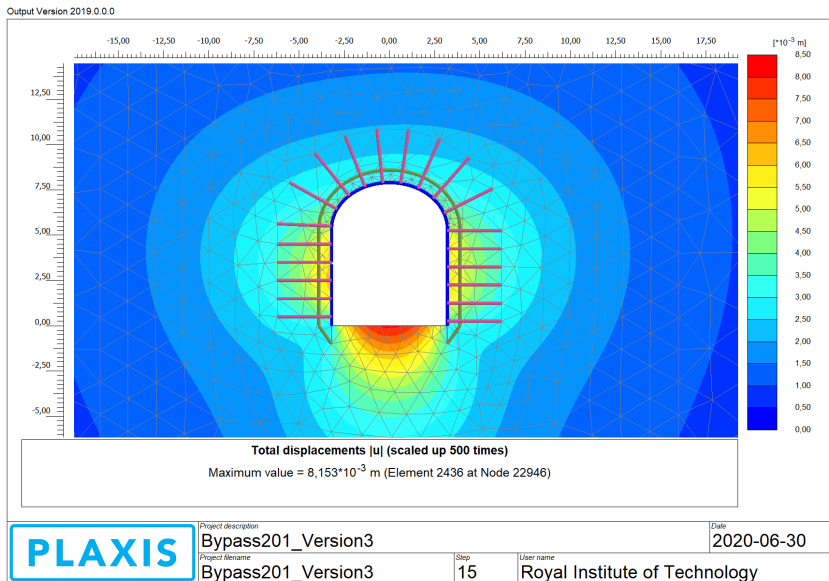


Figure 42 Shading of total deformation in stage 4

## Appendix B

Simplex in each round

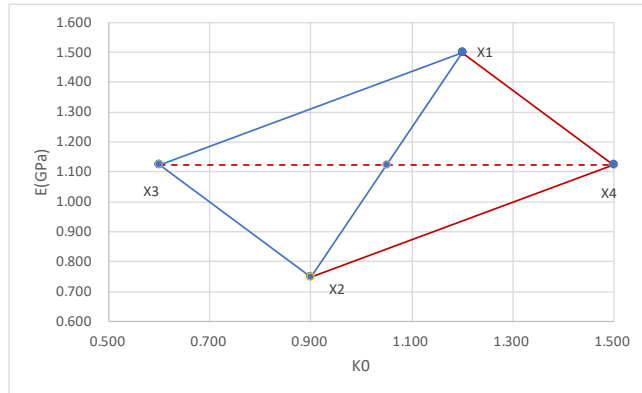


Figure 43 Simplex of round 1

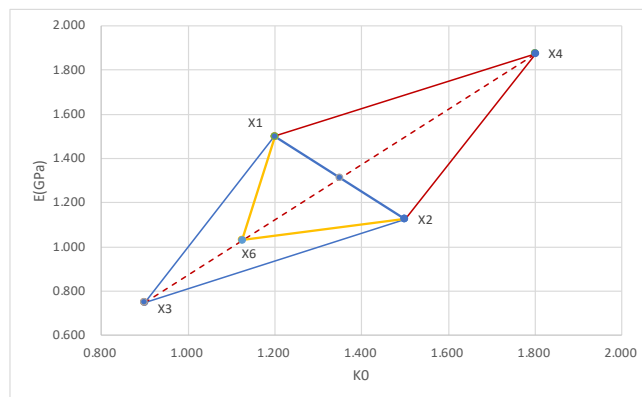


Figure 44 Simplex of round 2

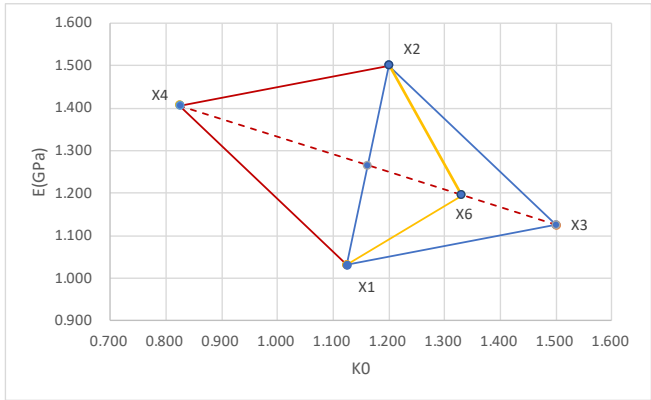


Figure 45 Simplex of round 3

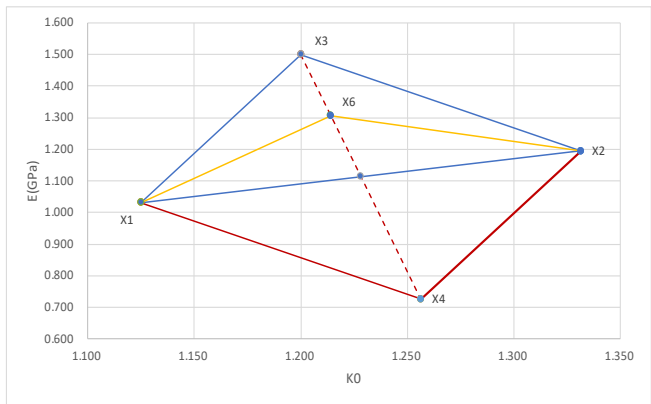


Figure 46 Simplex of round 4

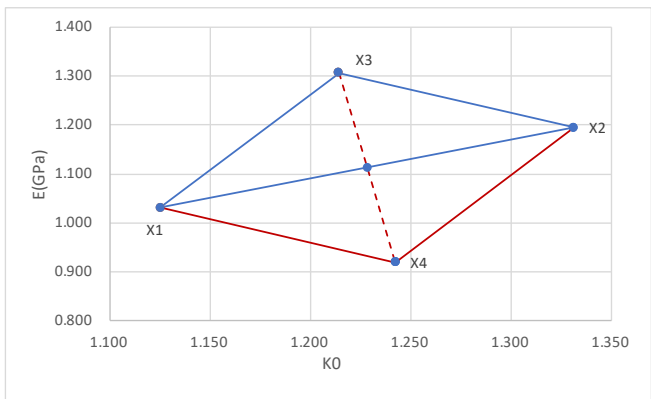


Figure 47 Simplex of round 5

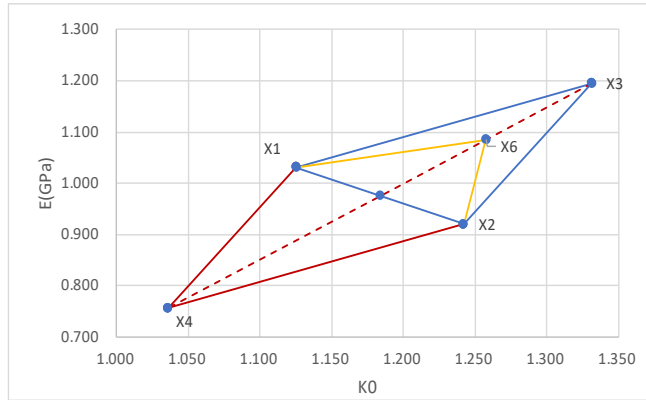


Figure 48 Simplex of round 6

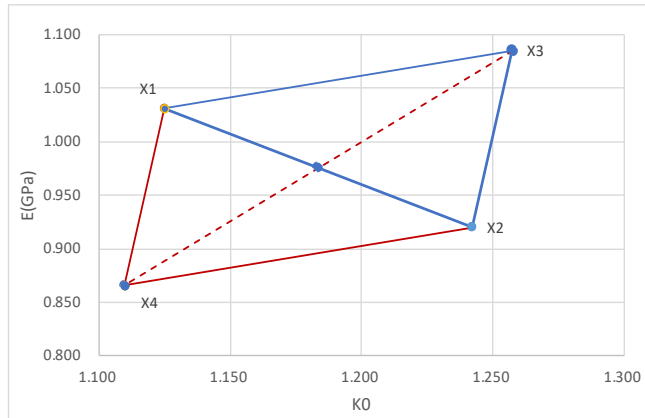


Figure 49 Simplex of round 7

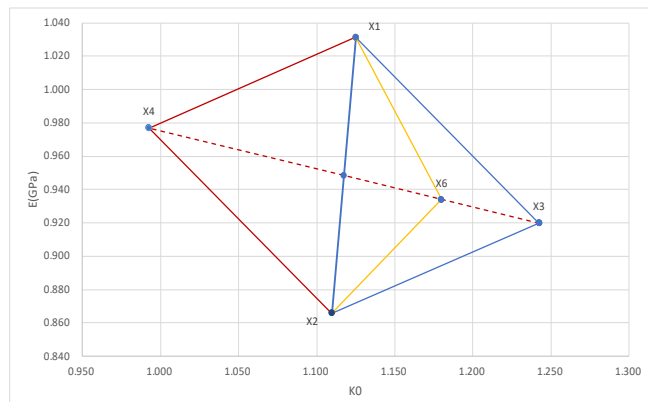


Figure 50 Simplex of round 8

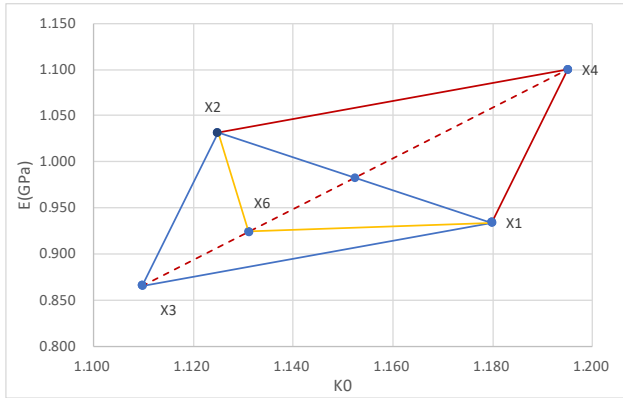


Figure 51 Simplex of round 9

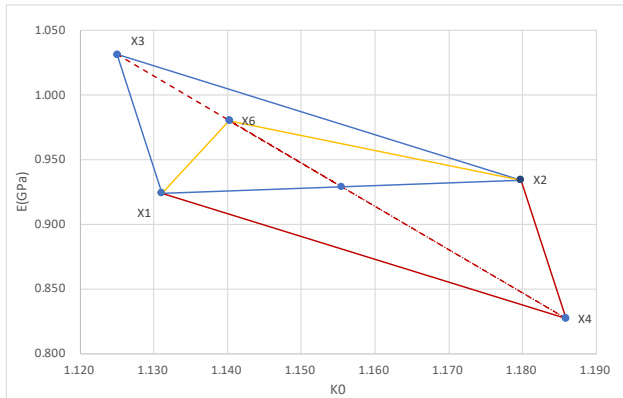


Figure 52 Simplex of round 10

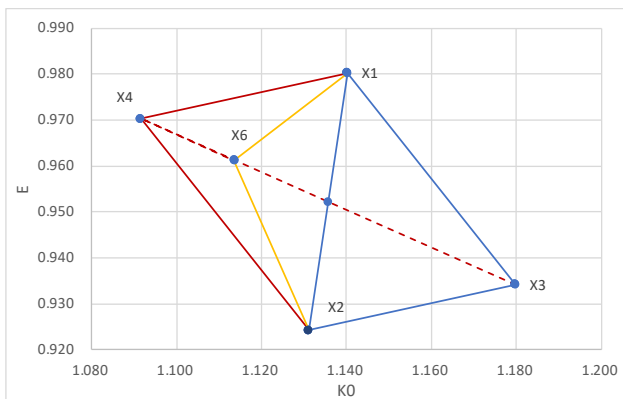


Figure 53 Simplex of round 11

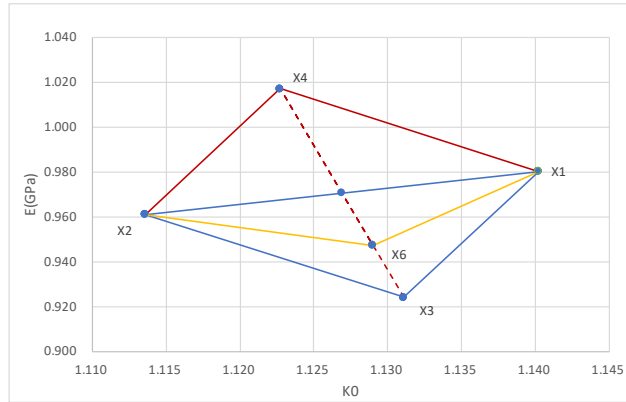


Figure 54 Simplex of round 12

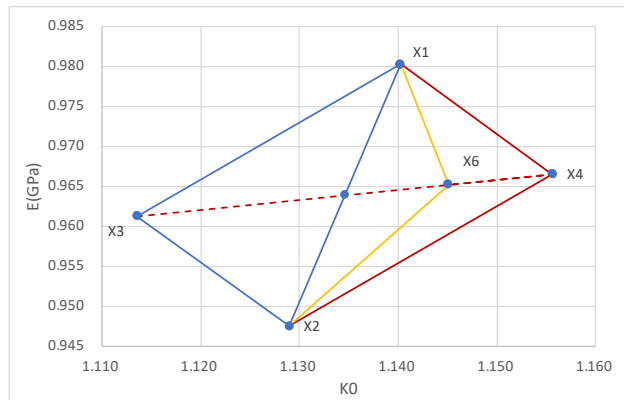


Figure 55 Simplex of round 13

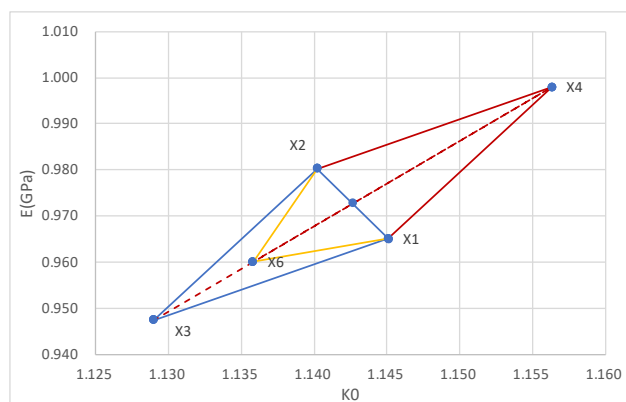


Figure 56 Simplex of round 14

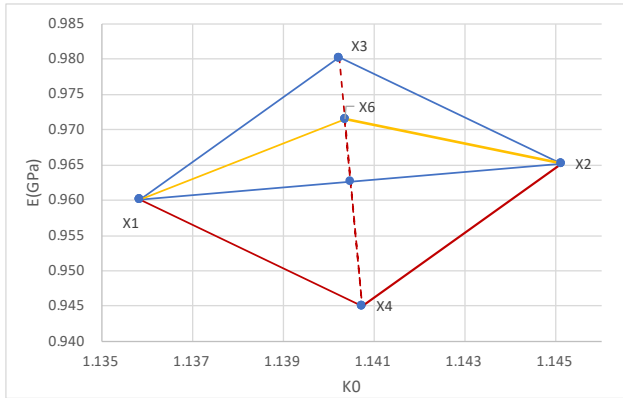


Figure 57 Simplex of round 15

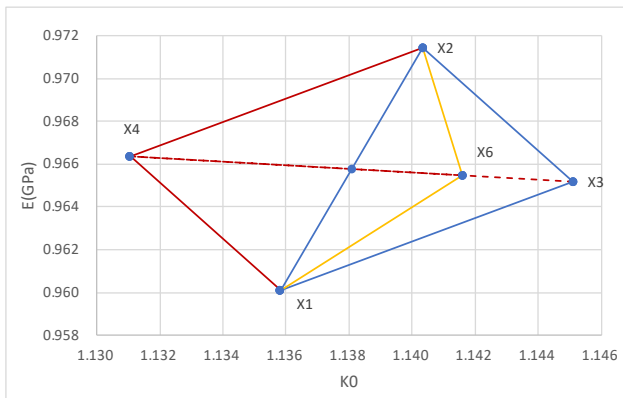


Figure 58 Simplex of round 16

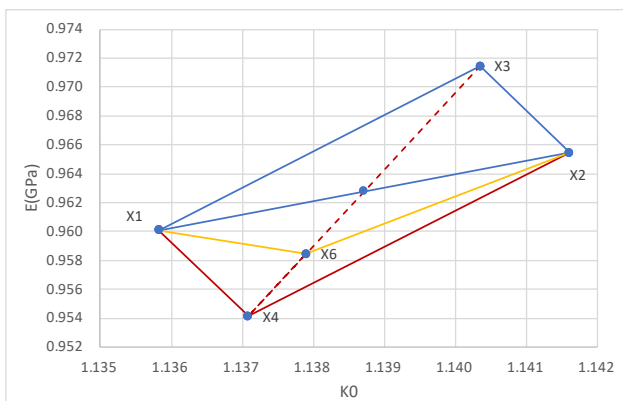


Figure 59 Simplex of round 17

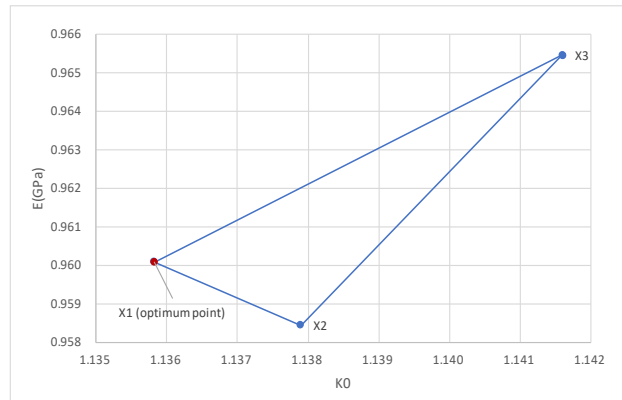


Figure 60 Final simplex

# Appendix C

## Results and search path of simplex method in sensitivity analysis

Table 14 Results of simplex method with initial deformation increasing 10%

	K0	E(GPa)	f1(mm)	f2(mm)	f3(mm)	U1	U2	U3	error
<b>Round1</b>									
X1	1.200	1.500	6.661	1.849	6.516	9.3	2.9	9.3	0.10049
X2	0.900	0.750	8.665	5.322	8.582	9.3	2.9	9.3	0.23605
X3	0.600	1.125	3.453	4.653	3.364	9.3	2.9	9.3	0.38936
middle point of X1X2	1.050	1.125							
X4	1.500	1.125	11.442	1.339	11.292	9.3	2.9	9.3	0.12956
<b>Round2</b>									
X1	1.200	1.500	6.661	1.849	6.516	9.3	2.9	9.3	0.10049
X2	1.500	1.125	11.442	1.339	11.292	9.3	2.9	9.3	0.12956
X3	0.900	0.750	8.665	5.322	8.582	9.3	2.9	9.3	0.23605
middle point of X1X2	1.350	1.313							
X4	1.800	1.875	8.986	0.046	8.940	9.3	2.9	9.3	0.32372
X6	1.125	1.031	8.735	3.000	8.558	9.3	2.9	9.3	0.00375
<b>Round3</b>									
X1	1.125	1.031	8.735	3.000	8.558	9.3	2.9	9.3	0.00375
X2	1.200	1.500	6.661	1.849	6.516	9.3	2.9	9.3	0.10049
X3	1.500	1.125	11.442	1.339	11.292	9.3	2.9	9.3	0.12956
middle point of X1X2	1.163	1.266							
X4	0.825	1.406	4.322	3.062	4.266	9.3	2.9	9.3	0.19421
X6	1.331	1.195	9.311	1.859	9.145	9.3	2.9	9.3	0.04305
<b>Round4</b>									
X1	1.125	1.031	8.735	3.000	8.558	9.3	2.9	9.3	0.00375
X2	1.331	1.195	9.311	1.859	9.145	9.3	2.9	9.3	0.04305
X3	1.200	1.500	6.661	1.849	6.516	9.3	2.9	9.3	0.10049
middle point of X1X2	1.228	1.113							
X4	1.256	0.727	13.933	3.600	14.027	9.3	2.9	9.3	0.18826
X6	1.214	1.307	7.679	2.077	7.521	9.3	2.9	9.3	0.04917
<b>Round5</b>									
X1	1.125	1.031	8.735	3.000	8.558	9.3	2.9	9.3	0.00375
X2	1.331	1.195	9.311	1.859	9.145	9.3	2.9	9.3	0.04305
X3	1.214	1.307	7.679	2.077	7.521	9.3	2.9	9.3	0.04917
middle point of X1X2	1.228	1.113							
X4	1.242	0.920	10.910	2.839	10.721	9.3	2.9	9.3	0.01792
<b>Round6</b>									
X1	1.125	1.031	8.735	3.000	8.558	9.3	2.9	9.3	0.00375
X2	1.242	0.920	10.910	2.839	10.721	9.3	2.9	9.3	0.01792
X3	1.331	1.195	9.311	1.859	9.145	9.3	2.9	9.3	0.04305
middle point of X1X2	1.184	0.976							
X4	1.036	0.756	10.485	4.594	10.271	9.3	2.9	9.3	0.12278
X6	1.257	1.085	9.498	2.338	9.330	9.3	2.9	9.3	0.01267
<b>Round7</b>									
X1	1.125	1.031	8.735	3.000	8.558	9.3	2.9	9.3	0.00375
X2	1.257	1.085	9.498	2.338	9.330	9.3	2.9	9.3	0.01267
X3	1.242	0.920	10.910	2.839	10.721	9.3	2.9	9.3	0.01792
middle point of X1X2	1.191	1.058							
X4	1.140	1.197	7.728	2.529	7.569	9.3	2.9	9.3	0.02653
X6	1.217	0.989	9.987	2.743	9.795	9.3	2.9	9.3	0.00374
<b>Round8</b>									
X1	1.217	0.989	9.987	2.743	9.795	9.3	2.9	9.3	0.00374
X2	1.125	1.031	8.735	3.000	8.558	9.3	2.9	9.3	0.00375
X3	1.257	1.085	9.498	2.338	9.330	9.3	2.9	9.3	0.01267
middle point of X1X2	1.171	1.010							
X4	1.084	0.935	9.127	3.492	8.940	9.3	2.9	9.3	0.01451
X6	1.214	1.048	9.436	2.597	9.251	9.3	2.9	9.3	0.00372

Round9									
X1	1.214	1.048	9.436	2.597	9.251	9.3	2.9	9.3	0.00372
X2	1.217	0.989	9.987	2.743	9.795	9.3	2.9	9.3	0.00374
X3	1.125	1.031	8.735	3.000	8.558	9.3	2.9	9.3	0.00375
middle point of X1X2	1.215	1.018							
X4	1.306	1.006	10.671	2.324	10.492	9.3	2.9	9.3	0.02587
X6	1.170	1.025	9.211	2.835	9.028	9.3	2.9	9.3	0.00048
Round10									
X1	1.170	1.025	9.211	2.835	9.028	9.3	2.9	9.3	0.00048
X2	1.214	1.048	9.436	2.597	9.251	9.3	2.9	9.3	0.00372
X3	1.217	0.989	9.987	2.743	9.795	9.3	2.9	9.3	0.00374
middle point of X1X2	1.192	1.036							
X4	1.168	1.084	8.727	2.685	8.550	9.3	2.9	9.3	0.00527
X6	1.204	1.013	9.641	2.730	9.452	9.3	2.9	9.3	0.00168
Round11									
X1	1.170	1.025	9.211	2.835	9.028	9.3	2.9	9.3	0.00048
X2	1.204	1.013	9.641	2.730	9.452	9.3	2.9	9.3	0.00168
X3	1.214	1.048	9.436	2.597	9.251	9.3	2.9	9.3	0.00372
middle point of X1X2	1.187	1.019							
X4	1.161	0.990	9.425	2.975	9.238	9.3	2.9	9.3	0.00030
X5	1.158	0.987	9.423	2.997	9.235	9.3	2.9	9.3	0.00045
Round12									
X1	1.161	0.990	9.425	2.975	9.238	9.3	2.9	9.3	0.00030
X2	1.170	1.025	9.211	2.835	9.028	9.3	2.9	9.3	0.00048
X3	1.204	1.013	9.641	2.730	9.452	9.3	2.9	9.3	0.00168
middle point of X1X2	1.165	1.007							
X4	1.126	1.002	8.979	3.084	8.798	9.3	2.9	9.3	0.00271
X6	1.185	1.010	9.482	2.816	9.295	9.3	2.9	9.3	0.00041
Round13									
X1	1.161	0.990	9.425	2.975	9.238	9.3	2.9	9.3	0.00030
X2	1.185	1.010	9.482	2.816	9.295	9.3	2.9	9.3	0.00041
X3	1.170	1.025	9.211	2.835	9.028	9.3	2.9	9.3	0.00048
middle point of X1X2	1.173	1.000							
X4	1.175	0.975	9.697	2.962	9.508	9.3	2.9	9.3	0.00093
X6	1.171	1.012	9.330	2.868	9.145	9.3	2.9	9.3	0.00014
Round14									
X1	1.171	1.012	9.330	2.868	9.145	9.3	2.9	9.3	0.00014
X2	1.161	0.990	9.425	2.975	9.238	9.3	2.9	9.3	0.00030
X3	1.185	1.010	9.482	2.816	9.295	9.3	2.9	9.3	0.00041
middle point of X1X2	1.166	1.001							
X4	1.147	0.992	9.270	3.027	9.084	9.3	2.9	9.3	0.00082
X6	1.175	1.006	9.420	2.869	9.232	9.3	2.9	9.3	0.00011
Round15									
X1	1.175	1.006	9.420	2.869	9.232	9.3	2.9	9.3	0.00011
X2	1.171	1.012	9.330	2.868	9.145	9.3	2.9	9.3	0.00014
X3	1.161	0.990	9.425	2.975	9.238	9.3	2.9	9.3	0.00030
middle point of X1X2	1.173	1.009							
X4	1.186	1.028	9.338	2.761	9.153	9.3	2.9	9.3	0.00085
X6	1.167	0.999	9.403	2.922	9.217	9.3	2.9	9.3	0.00009
The final simplex									
X1	1.167	0.999	9.403	2.922	9.217	9.3	2.9	9.3	0.00009
X2	1.175	1.006	9.420	2.869	9.232	9.3	2.9	9.3	0.00011
X3	1.171	1.012	9.330	2.868	9.145	9.3	2.9	9.3	0.00014

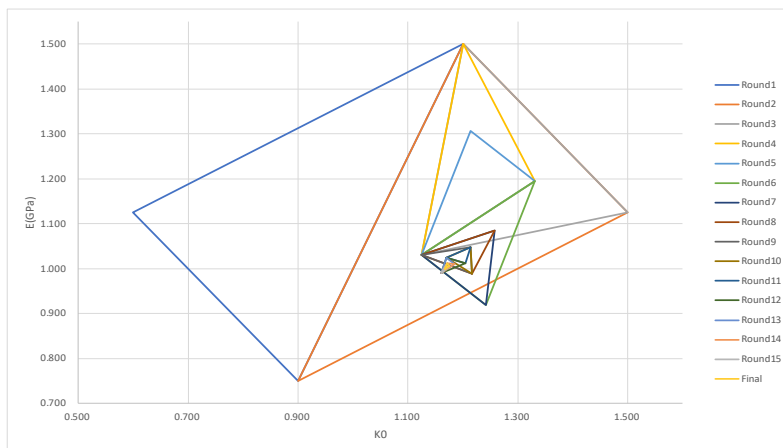


Figure 61 Search path of simplex method with initial deformation increasing 10%

Table 15 Results of simplex method with initial deformation decreasing 10%

	K0	E(GPa)	f1(mm)	f2(mm)	f3(mm)	U1	U2	U3	error
Round1									
X1	1.200	1.500	6.689	1.566	6.632	9.3	2.9	9.3	0.12424
X2	0.900	0.750	8.610	4.704	8.204	9.3	2.9	9.3	0.13545
X3	0.600	1.125	3.277	4.219	3.039	9.3	2.9	9.3	0.35984
middle point of X1X2	1.050	1.125							
X4	1.500	1.125	11.370	0.936	11.397	9.3	2.9	9.3	0.18635
X6	1.275	1.125	9.290	1.770	9.087	9.3	2.9	9.3	0.05079
Round2									
X1	1.275	1.125	9.290	1.770	9.087	9.3	2.9	9.3	0.05079
X2	1.200	1.500	6.689	1.566	6.632	9.3	2.9	9.3	0.12424
X3	0.900	0.750	8.610	4.704	8.204	9.3	2.9	9.3	0.13545
middle point of X1X2	1.238	1.313							
X4	1.575	1.875	7.584	0.388	7.469	9.3	2.9	9.3	0.27437
X6	1.069	1.031	8.083	2.771	8.027	9.3	2.9	9.3	0.01261
Round3									
X1	1.069	1.031	8.083	2.771	8.027	9.3	2.9	9.3	0.01261
X2	1.275	1.125	9.290	1.770	9.087	9.3	2.9	9.3	0.05079
X3	1.200	1.500	6.689	1.566	6.632	9.3	2.9	9.3	0.12424
middle point of X1X2	1.172	1.078							
X4	1.144	0.656	13.175	3.926	12.857	9.3	2.9	9.3	0.14836
X6	1.186	1.289	7.550	1.842	7.395	9.3	2.9	9.3	0.07016
Round4									
X1	1.069	1.031	8.083	2.771	8.027	9.3	2.9	9.3	0.01261
X2	1.275	1.125	9.290	1.770	9.087	9.3	2.9	9.3	0.05079
X3	1.186	1.289	7.550	1.842	7.395	9.3	2.9	9.3	0.07016
middle point of X1X2	1.172	1.078							
X4	1.158	0.867	10.437	2.867	10.141	9.3	2.9	9.3	0.00775
X5	1.156	0.846	10.637	2.948	10.340	9.3	2.9	9.3	0.01115
Round5									
X1	1.158	0.867	10.437	2.867	10.141	9.3	2.9	9.3	0.00775
X2	1.069	1.031	8.083	2.771	8.027	9.3	2.9	9.3	0.01261
X3	1.275	1.125	9.290	1.770	9.087	9.3	2.9	9.3	0.05079
middle point of X1X2	1.113	0.949							
X4	0.952	0.773	9.015	4.297	8.646	9.3	2.9	9.3	0.07931
X6	1.194	1.037	9.251	2.247	8.968	9.3	2.9	9.3	0.01733
Round6									
X1	1.158	0.867	10.437	2.867	10.141	9.3	2.9	9.3	0.00775
X2	1.069	1.031	8.083	2.771	8.027	9.3	2.9	9.3	0.01261
X3	1.194	1.037	9.251	2.247	8.968	9.3	2.9	9.3	0.01733
middle point of X1X2	1.113	0.949							
X4	1.032	0.861	9.100	3.487	8.816	9.3	2.9	9.3	0.01471
X6	1.073	0.905	9.169	3.136	8.895	9.3	2.9	9.3	0.00291
Round7									
X1	1.073	0.905	9.169	3.136	8.895	9.3	2.9	9.3	0.00291
X2	1.158	0.867	10.437	2.867	10.141	9.3	2.9	9.3	0.00775
X3	1.069	1.031	8.083	2.771	8.027	9.3	2.9	9.3	0.01261
middle point of X1X2	1.115	0.886							
X4	1.162	0.741	12.031	3.352	11.697	9.3	2.9	9.3	0.05899
X6	1.097	0.944	9.056	2.908	8.996	9.3	2.9	9.3	0.00059
Round8									
X1	1.097	0.944	9.056	2.908	8.996	9.3	2.9	9.3	0.00059
X2	1.073	0.905	9.169	3.136	8.895	9.3	2.9	9.3	0.00291
X3	1.158	0.867	10.437	2.867	10.141	9.3	2.9	9.3	0.00775
middle point of X1X2	1.085	0.925							
X4	1.012	0.982	7.892	3.133	7.594	9.3	2.9	9.3	0.02101
X6	1.121	0.896	9.734	2.942	9.450	9.3	2.9	9.3	0.00088
Round9									
X1	1.097	0.944	9.056	2.908	8.996	9.3	2.9	9.3	0.00059
X2	1.121	0.896	9.734	2.942	9.450	9.3	2.9	9.3	0.00088
X3	1.073	0.905	9.169	3.136	8.895	9.3	2.9	9.3	0.00291
middle point of X1X2	1.109	0.920							
X4	1.145	0.935	9.621	2.712	9.348	9.3	2.9	9.3	0.00181
X6	1.127	0.928	9.497	2.812	9.222	9.3	2.9	9.3	0.00048

Round10									
X1	1.127	0.928	9.497	2.812	9.222	9.3	2.9	9.3	0.00048
X2	1.097	0.944	9.056	2.908	8.996	9.3	2.9	9.3	0.00059
X3	1.121	0.896	9.734	2.942	9.450	9.3	2.9	9.3	0.00088
middle point of X1X2	1.112	0.936							
X4	1.102	0.976	8.835	2.777	8.562	9.3	2.9	9.3	0.00353
X6	1.117	0.916	9.499	2.894	9.216	9.3	2.9	9.3	0.00018
Round11									
X1	1.117	0.916	9.499	2.894	9.216	9.3	2.9	9.3	0.00018
X2	1.127	0.928	9.497	2.812	9.222	9.3	2.9	9.3	0.00048
X3	1.097	0.944	9.056	2.908	8.996	9.3	2.9	9.3	0.00059
middle point of X1X2	1.122	0.922							
X4	1.147	0.899	10.002	2.815	9.699	9.3	2.9	9.3	0.00280
X6	1.109	0.933	9.261	2.875	8.979	9.3	2.9	9.3	0.00043
Round12									
X1	1.117	0.916	9.499	2.894	9.216	9.3	2.9	9.3	0.00018
X2	1.109	0.933	9.261	2.875	8.979	9.3	2.9	9.3	0.00043
X3	1.127	0.928	9.497	2.812	9.222	9.3	2.9	9.3	0.00048
middle point of X1X2	1.113	0.924							
X4	1.099	0.921	9.265	2.957	8.976	9.3	2.9	9.3	0.00054
X6	1.120	0.926	9.439	2.849	9.159	9.3	2.9	9.3	0.00025
Round13									
X1	1.117	0.916	9.499	2.894	9.216	9.3	2.9	9.3	0.00018
X2	1.120	0.926	9.439	2.849	9.159	9.3	2.9	9.3	0.00025
X3	1.109	0.933	9.261	2.875	8.979	9.3	2.9	9.3	0.00043
middle point of X1X2	1.118	0.921							
X4	1.127	0.909	9.674	2.873	9.397	9.3	2.9	9.3	0.00060
X6	1.114	0.927	9.367	2.872	9.086	9.3	2.9	9.3	0.00022
Round14									
X1	1.117	0.916	9.499	2.894	9.216	9.3	2.9	9.3	0.00018
X2	1.114	0.927	9.367	2.872	9.086	9.3	2.9	9.3	0.00022
X3	1.120	0.926	9.439	2.849	9.159	9.3	2.9	9.3	0.00025
middle point of X1X2	1.115	0.921							
X4	1.110	0.917	9.416	2.922	9.132	9.3	2.9	9.3	0.00018
Round15									
X1	1.117	0.916	9.499	2.894	9.216	9.3	2.9	9.3	0.00018
X2	1.110	0.917	9.416	2.922	9.132	9.3	2.9	9.3	0.00018
X3	1.114	0.927	9.367	2.872	9.086	9.3	2.9	9.3	0.00022
middle point of X1X2	1.113	0.916							
X4	1.113	0.906	9.550	2.945	9.265	9.3	2.9	9.3	0.00033
X6	1.114	0.922	9.412	2.888	9.129	9.3	2.9	9.3	0.00017
Round16									
X1	1.114	0.922	9.412	2.888	9.129	9.3	2.9	9.3	0.00017
X2	1.117	0.916	9.499	2.894	9.216	9.3	2.9	9.3	0.00018
X3	1.110	0.917	9.416	2.922	9.132	9.3	2.9	9.3	0.00018
middle point of X1X2	1.115	0.919							
X4	1.120	0.921	9.484	2.865	9.204	9.3	2.9	9.3	0.00021
X6	1.113	0.918	9.438	2.905	9.155	9.3	2.9	9.3	0.00016
The final simplex									
X1	1.113	0.918	9.438	2.905	9.155	9.3	2.9	9.3	0.00016
X2	1.114	0.922	9.412	2.888	9.129	9.3	2.9	9.3	0.00017
X3	1.117	0.916	9.499	2.894	9.216	9.3	2.9	9.3	0.00018

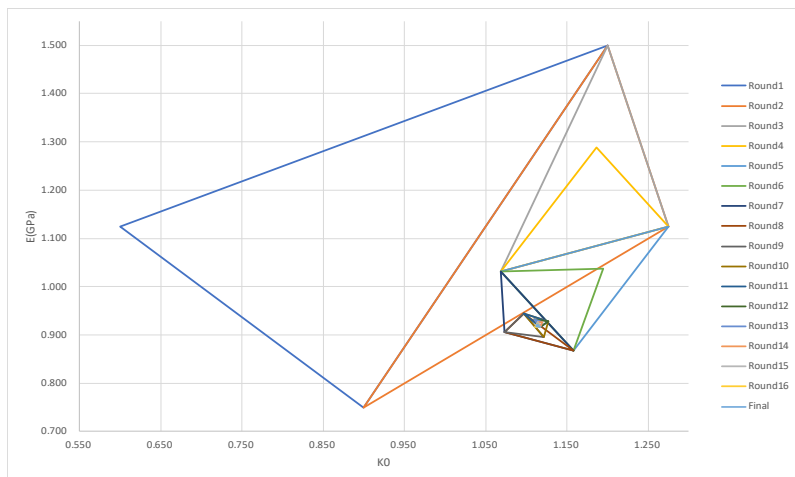


Figure 62 Results of simplex method with initial deformation decreasing 10%

TRITA-ABE-MBT-22588

[www.kth.se](http://www.kth.se)

---